1-1-1978

Creep and deformation maps for alpha and beta zirconium.

Satish D. Patel

CREEP AND DEFORMATION MAPS FOR α AND β ZIRCONIUM

by

Satish D. Patel

A Thesis
Presented to the Graduate Committee
of Lehigh University
in Candidacy for the Degree of
Master of Science
in
Metallurgy and Materials Science

Lehigh University
1978

This thesis is accepted and approved in partial fulfillment of the requirements for the degree of Master of Science.

July 18, 1978

(date)

Professor in Charge

Chairman of Department

ACKNOWLEDGEMENTS

The completion of this research would have been impossible without the encouragement of Dr. M. R. Notis. In addition to technical guidance his patience proved invaluable.

Thanks also to Dr. M. F. Ashby whose constructive criticism during the final planning of the research was much appreciated. Special thanks must go to Carlos Vinante for his assistance in the preparation of the computer program.

Additional credit must be extended to Dr. V. Krishnamachari for help with the creep testing machine. My fellow graduate students, especially Bruce Smith, Ravi Verma, R. Vasudevan, and Steve Young, must be thanked for their assistance in completing the work.

TABLE OF CONTENTS

LIST OF FIGURES

LIST OF TABLES

ABSTRACT

Deformation mechanism maps have been developed and include various theoretical models characterizing the peculiar creep deformation properties of zirconium. The "Mixed Glide and Diffusion Control" model (explaining the anomalous stress dependence of zirconium) developed by Ardell and Sherby explains the behavior of the low temperature α - (h. c. p.) phase adequately. Difficulties encountered in trying to incorporate models explaining the plateau in the yield stress versus temperature curve are discussed. Temperatures above the α - β phase transformation have been included in the maps; the properties of the β - (b. c. c.) phase pose difficulties due to its anomalous self-diffusion behavior. Due to the lack of literature on the mechanical properties of β - zirconium, the maps were developed on the assumption that its behavior is similar to "normal" b. c. c. metals. Constant - stress, compressive creep tests were conducted from 900°C to 1200°C over the stress range of 2.7 MPa to 31.0 MPa to test the validity of the map for β - zirconium; similarly, comparison is made between predicted creep rate values and those observed in a number of previously published experimental studies. Finally, a description is given of initial approaches to the incorporation of irradiation creep effects in the map.

1. INTRODUCTION

Zirconium and its alloys are commonly used as fuel cladding materials in light water and boiling water reactors. Similarly, zirconium and its alloys are used as structural members in the reactor core and in the primary steam generation equipment. In any of these applications the material is bound to undergo inelastic deformation under the complex stress history and hostile environment of a reactor.

Although zirconium has been used for a considerable time, there exists no adequate understanding of its mechanical properties. A general overview of the creep properties of alpha zirconium has been presented by Knorr and Notis [1]. However, some of the important peculiarities of zirconium do not appear on the initial deformation maps originated by Knorr and Notis. Therefore, high temperature properties cannot be predicted from extrapolated data with sufficient accuracy. Also, difficulties are encountered, such as the $\alpha \rightarrow \beta$ transformation at 862°C which makes extrapolation erroneous. At lower temperatures zirconium is thought to deform by a mixed glide and climb mechanism [2] which does not seem to found in most materials. Thus titanium which is structurally similar to zirconium shows "normal" low temperature behavior while zirconium does not. Also, in the temperature range of 300°C to 800°C a plateau in the yield strength versus temperature curve is observed. There are a number of different models proposed to explain this

plateau. Heritier et al. [3] believe it to be related to an athermal plastic flow mechanism, while Miller and Sherby [4] have offered a reasonable explanation based completely on a thermally activated approach.

This thesis attempts to incorporate the peculiar deformation behavior of zirconium into a general model. Although there is sufficient creep data in the literature for alpha-zirconium no creep data exist for beta-zirconium. Prediction of the creep properties of beta-zirconium from extrapolated data on alpha-zirconium is difficult because of the presence of a phase transformation and because of the unusual deformation behavior of the alpha-phase. The purpose of this thesis is, therefore, to develop an extensive computer modeling or "deformation mapping" approach that will provide a more reasonable means for the extrapolation and prediction of the creep behavior of this material. The validity of this approach is confirmed through the comparison of the theoretically predicted and experimentally measured creep behavior of beta-zirconium.

2. DEFORMATION MECHANISMS - A GENERAL APPROACH

The application of dislocation and rate theories to the study of the continuing plastic deformation of materials subjected to a constant load (or constant stress) is probably the main reason for the considerable progress that has been made over the recent past

in this field. It has led to the formulation of rate equations for the physical mechanisms that take place in materials. Because of the great versatility of dislocations and the numerous interactions they may undertake with one another and with vacancies and grain boundaries, a number of different mechanisms can control creep. These mechanisms can be classified as "Series" (concurrent) or "Parallel" (sequential) depending on whether they operate independently of one another or not. These processes when added together account for the experimental deformation obtained within a reasonable degree of accuracy.

The contribution of each mechanism depends on the nature of the simultaneous processes. Two or more processes taking place simultaneously can operate either in parallel or in series. For example, diffusional creep can take place by volume or boundary diffusion and each can operate independently of the other. The observed rate is therefore:

$$r = r_1 + r_2 \tag{2.1}$$

These are considered as series processes. On the other hand, simultaneous processes may be interdependent. For example, a dislocation may have to over come several obstacles (solute particles, forest dislocations, internal stress fields) before it produces macroscopic strain due to glide. Also, the activation energy will be altered due to interactions between the various processes.

However, in the ideal case in which the time spent at each obstacle is independent of the presence of other obstacles, the total time required for a dislocation to travel a certain large distance is the sum of all the waiting times at the various obstacles. In such an ideal case, the reciprocal strain rate is the sum of the individual rates:

$$1/r = 1/r_1 + 1/r_2 \tag{2.2}$$

These are considered as parallel processes. It is clear from the above that the strain rate produced when two or more processes interact in this manner is dependent upon the slowest step in the process. The strain rate in a series process is dependent upon the most rapid step in the process.

For each mechanism there is usually a strain-rate equation. In its simplest form it is:

$$\dot{\varepsilon} = f(\sigma, T, \text{Structure}) \tag{2.3}$$

where

$\dot{\varepsilon}$ = Strain-rate*

σ = Applied stress

T = Temperature under consideration

*Strains and strain rates in this equation are tensile, the corresponding shear terms may be found from relations of the form $\dot{\gamma} = \sqrt{3}\,\dot{\varepsilon}$.

a mathematical relationship which gives us the strain-rate as a function of stress, temperature, and structure. There are a number of structural parameters such as grain size, solute or precipitate concentration, dislocation density, crystal class, type of bonding, etc., so that the complete form of the equation may look like:

$$\dot{\varepsilon} = f(\sigma, T, S_1, S_2, S_3.....) \tag{2.4}$$

If a convenient, simplified form of the above equation is needed, it usually becomes necessary to make assumptions. Thus, to have a relationship between $\dot{\varepsilon}$, σ, and T, the internal structure needs simplification. In order to do this, one needs to make one of the following assumptions.

a. Steady-State Flow: This assumes that structural parameters, such as dislocation density, no longer appear in the rate equation explicitly. They take on unique values determined by the conditions of stress and temperature. In effect, we are setting:

$$dS_1 = dS_2 = dS_3 ..... = 0 \tag{2.5}$$

and solving for S_1, S_2, S_3 in terms of σ and T.

b. A Constant Internal Structure: This assumes that structural parameters, such as dislocation density, grain size, etc., are assumed constant, so that equation (2.4) reduces to:

$$\dot{\varepsilon} = f(\sigma,T) \tag{2.6}$$

This requires that the parameters S_1, S_2, S_3..... be known or specified.

Generally, according to Frost and Ashby [5], high temperature deformation is described by the steady state formulation, and low temperature deformation is commonly characterized by constant internal structure. In fact, a steady state deformation is rarely measured at low temperatures because of work hardening effects.

3. DEFORMATION IN NORMAL SOLIDS

It has now been firmly established that creep of crystalline solids occurs as a result of thermally activated migration of dislocations, grain boundary shearing and diffusion of vacancies. Because of the great versatility of dislocations and the numerous interactions they may undergo with one another, with additional lattice defects and various substructural details, a number of different mechanisms can control creep. At low temperatures, because the dislocations are not sufficiently activated, only the lowest energy barriers are crossed. As they pass over these, the dislocations are met by higher energy barriers which impede their motion. Consequently, low temperature creep is characterized by a decreasing creep rate. At sufficiently high stresses, dislocations may surmount most barriers and may glide through the lattice.

At somewhat higher temperatures, the dislocations are sufficiently stimulated to overcome the low energy barriers more fre-

quently. At this stage, a larger apparent initial creep strain is observed for the same applied stress level. Also, if the temperature is greater than about $T_M/2$, creep continues to take place despite the fact that the gliding dislocations have been arrested. The reason for this being that it is above $T_M/2$ that diffusion first becomes appreciable. Dislocations now acquire a new degree of freedom such that edge components of dislocations are no longer confined to glide exclusively on their original slip planes and may climb to new planes. This is normally known to occur at fairly high stresses and high temperatures (above 0.5 T_M).

If the applied stress is relatively low, each dislocation is not able to move as a "unit" and creep is generally believed to be due to a stress-directed atom migration process. This type of deformation is known as diffusional creep.* (For example, Nabarro-Herring [6] and Coble [7] creep.)

The above are the commonly known modes of plastic deformation. These processes are independent and distinguishable from each other. Some of the other processes of plastic flow include: (i) deformation by twinning, (ii) athermal flow at low temperatures, and (iii) radiation creep in reactor environments.

These processes are known to occur in most metals, but are

*Ashby [8] has recently shown that identical creep equations can be derived using grain boundary dislocation models rather than the traditional stress-directed vacancy flow picture.

extremely elusive when one attempts to quantitatively model them with a reasonable degree of accuracy.

Although an in-depth study of each of the creep mechanisms is beyond the scope of this thesis, a short paragraph on the salient features of each is needed in order to look at them in a better perspective.

a. Nabarro-Herring Creep

This type of creep results from the diffusion of vacancies through the bulk lattice from regions of high chemical potential at grain boundaries subjected to normal tensile stresses to regions of lower chemical potential at grain boundaries in compression. Atom migration in the opposite direction accounts for the creep strain.

Mathematically, the steady-state creep (strain) rate due to Nabarro-Herring [6] creep is given by:

$$\dot{\varepsilon}_{NH} = \frac{13.3\ D_V \Omega \sigma}{KT\ d^2} \tag{3.1}$$

where

σ = applied stress

D_V = lattice diffusion coefficient

Ω = atomic volume

d = grain size

K = Boltzmann's constant

T = absolute temperature

In addition to yielding a linear relation between creep-rate and stress, the Nabarro-Herring model predicts that the steady state creep rate should be inversely proportional to the square of the grain diameter. Thus, a fine grain size specimen will creep faster than a coarse grain sample. Also, it has been established that this creep mechanism is valid only at low stresses where motion of dislocation is restricted and at temperatures greater than about $0.6\ T_M$ - $0.7\ T_M$.

b. Coble Creep

If the temperature is lower than approximately $0.6\ T_M$ - $0.7\ T_M$ grain boundary diffusion is likely to dominate over lattice diffusion. The atoms will no longer move through the bulk of the lattice; instead, shorter, faster paths through the grain boundaries will be preferred. For Coble creep [7] the strain rate is given by:

$$\dot{\varepsilon}_C = \frac{47.5\Omega(D_b \cdot W)\sigma}{KT\, d^3} \qquad (3.2)$$

where $D_b \cdot W$ is the product of the grain boundary diffusion coefficient and the effective grain boundary width, respectively.

In actuality, diffusional flow is not quite as simple as described above. The equations for Coble [7] and Nabarro-Herring [6] creep are over-simplifications in that they neglect the kinetics

involved in detaching the vacancies from grain boundary sites and reattaching them again. This interface is pictured as a perfect source or sink for vacancies and the possibility of interface control is not included in the model. Although more recent work [9] has treated this problem, the simple more classical approaches are considered sufficiently accurate for the present research.

c. Dislocation Climb

The most generally accepted "semi-empirical" equation describing dislocation plastic flow controlled by climb is that developed by Mukherjee, Bird, and Dorn [10]:

$$\dot{\varepsilon} = \frac{AD_V \mu b}{KT} \left(\frac{\sigma}{\mu}\right)^n \qquad (3.3)$$

where

A = Dorn parameter*

μ = temperature dependent shear modulus

b = Burger's vector

n = stress exponent

D_V = volume diffusion coefficient.

The value of 'n' has been found to vary from 2 to 8 for most pure metals [11]. A broad correlation between 'n' and A for a wide variety of materials has been noted by Stocker and Ashby [11].

*For the Shear equation, Frost and Ashby [5] have shown that $A(\text{Shear}) = (\sqrt{3})^{n+1} A(\text{tensile})$.

The above equation is applicable in the stress range $0 < \sigma/\mu < 10^{-3}$ and holds for a wide variety of materials but it is not altogether satisfactory. No theoretical model can convincingly explain the observed values of 'n' and the large values of the dimensionless constant A. This suggests that some important physical quantity (subgrain size or stacking fault energy, for example) is missing from the equation (3.3) in the form presented here. Again, more formal equations, each assuming a specific dislocation geometry or interaction are available in the literature [12,13]. These were, however, not thought to be significantly more accurate for the purpose of the present work, especially since little or no information is available in the literature concerning dislocation structure and dynamics in Zr (i.e., good electron microscope studies are lacking).

Finally, Frost and Ashby [5] have recently shown that the diffusion term in equation (3.3) should be replaced by an <u>effective</u> diffusion term that includes the diffusion contribution due to diffusion along dislocation pipes at lower temperature. Thus, they suggest an equation of the form:

$$D_{eff} = D_V \left[1 + \frac{10A_c}{b^2} \left(\frac{\sigma}{\mu}\right)^2 \frac{D_C}{D_V}\right] \qquad (3.5)$$

where

A_C = cross-sectional area of the dislocation core

D_C = core diffusion coefficient

D_V = lattice diffusion coefficient

μ = temperature dependent shear modulus.

Considering the unusually large lattice diffusion observed for Zr [14] it is likely that the pipe diffusion contribution is suppressed for this material and may be ignored, at least as a first order effect.

d. Dislocation Glide

Flow by pure dislocation glide can be further subdivided on the basis of the type of resistance encountered in the solid:

i. Glide Limited by a Lattice Resistance

This type of glide is commonly referred to as "Peierls" Stress and is due to the dislocation's interaction with the atomic structure itself. In effect, the crystal lattice presents an array of infinitely long straight barriers to the motion of the dislocation, the dislocation advances by forming kink pairs which subsequently spread apart [15]. The rate equation based on this model is

$$\dot{\varepsilon} = \dot{\varepsilon}_p \left(\frac{\sigma}{\mu}\right)^2 \exp\left\{-\frac{\Delta F_K}{KT}\left[1 - (\sigma/T_p)^p\right]^q\right\} \qquad (3.6)$$

where

ΔF_K = Helmholtz free energy of an isolated pair of kinks

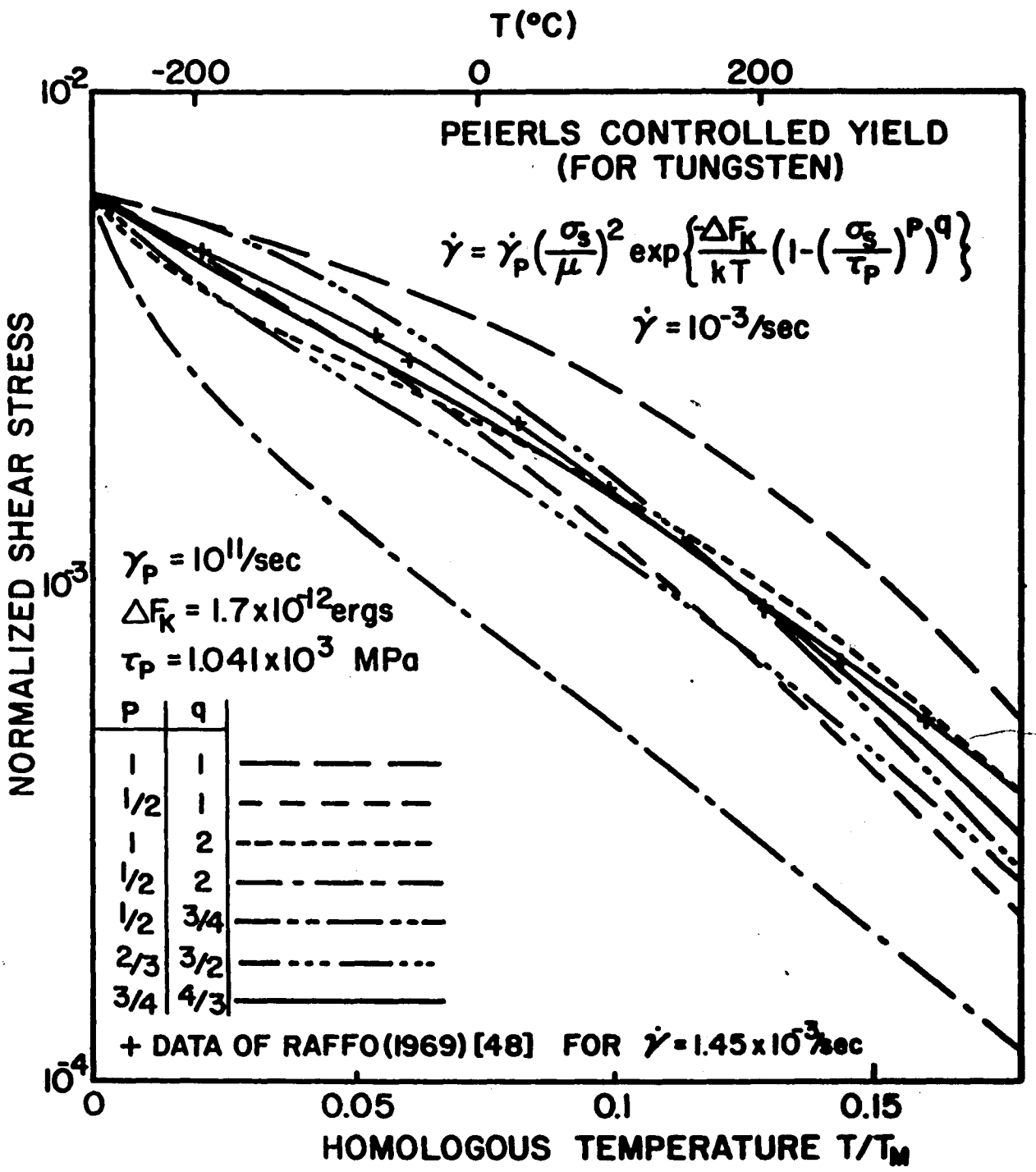

Fig.(3-1)- Contours for $\dot{\gamma}=10^{-4}$/sec for various formulations of the Peierls-controlled glide equation. Raffo (48)

τ_p = flow stress at 0°K

$\dot{\varepsilon}_p$ = constant with dimensions of strain rate

Frost and Ashby [5] have demonstrated that the above equation is extremely sensitive to the values of p and q, and they have calculated several sets of values for p and q (Figure 3-1). Although these contours do not overlap exactly, the shapes are similar, and they could be made to overlap well if the parameters $\dot{\varepsilon}_p$, ΔF_K, and τ_p were appropriately adjusted.

The values of ΔF_K (typically 0.1 to 1μb^3) and τ_p (typically 10^{-3} to $10^{-1}\mu$) which reflect the values of the interatomic forces are determined experimentally. The slope of the constant strain-rate contour shown in Figure 3-1 determines the value of ΔF_K whereas the value of τ_p is obtained by the intercept of the contour on the Y-axis. The pre-exponential contains a factor of stress squared, representing the variation of mobile dislocation density with stress. If one were to be more accurate, the variation of the steady state kink density with stress should be considered rather than the variation of mobile dislocation density. However, the problem is only partly resolved [16] due to a lack of experimental data, which prevents the treatment of the pre-exponential stress power as an adjustable parameter. Frost and Ashby [5] have shown that changing the power terms does not substantially change the maps, although a change in the value of $\dot{\varepsilon}_p$ would be required. In this present work, however, with the stress-

squared pre-exponential the value of $\dot{\varepsilon}_p = 10^{11}$/sec has been used.

ii. Glide Limited by Discrete Obstacle

The discrete obstacles normally encountered are other dislocations, solutes, precipitates and grain boundaries. The glide controlled flow rate limited by discrete obstacles also appears as an exponential function of stress [5,16,17]:

$$\dot{\varepsilon} = \dot{\varepsilon}_o \exp\left[-\frac{\Delta F}{KT}\left(1 - \frac{\sigma}{T_o}\right)\right] \tag{3.7}$$

where

T_o = flow stress in the absence of thermal activation ($\approx \frac{\mu b}{\ell}$, where ℓ = mean obstacle spacing)

ΔF = total free energy required to overcome an obstacle without aid from external stress; it depends on the obstacle strength

$\dot{\varepsilon}_o$ = constant with dimensions of strain-rate.

The values of ΔF (typically 0.1 to $1\mu b^3$) and T_o can be obtained experimentally as described before for $p = 1$ and $q = 1$. Assuming these values for p and q implies that the obstacles are box-shaped and regularly spaced [16]. However, the influence on the shape of the strain-rate contours is not great and is, therefore, sufficiently accurate for the present research. Neglecting the pre-exponential stress dependence also has little effect as shown

earlier, and in this work $\dot{\varepsilon}_0 = 10^6$/sec has been used.

iii. Glide Limited by Phonon or Other Drag

This mechanism of deformation is known to occur under conditions of explosive or shock loading. It, therefore, leads to large strain-rates and is limited by the interaction of a moving dislocation with electrons and phonons [18]. Although this mechanism has not been included in the maps for zirconium, another drag mechanism [19], due to solute atoms and involving lower strain rates has been considered. This will be discussed in detail later, in this chapter.

e. Defectless Flow

Loosely, this may be defined as the flow of a material when the ideal shear strength is exceeded. The ideal shear strength is the stress level above which flow of a defect-free crystal becomes catastrophic. Thus,

$$\dot{\gamma} = \infty \text{ when } \sigma \geq T \text{ theoretical} \tag{3.8}$$

and

$$\dot{\gamma} = 0 \text{ when } \sigma < T \text{ theoretical} \tag{3.9}$$

For b.c.c. metals, the theoretical shear strength is approximately 0.11μ as determined by MacKenzie [20] and for f.c.c. metals it is 0.6μ [20].

The above mechanisms are the ones that have been established and are known to occur in most metals. These are the mechanisms that would be included in a "normal" map. However, zirconium behaves abnormally (to be discussed in next section), therefore, the map for zirconium has to be modified and would look appropriately different. In addition to those mechanisms that should specifically be added for zirconium, a survey of the literature indicates that there are several mechanisms that could be missing: At low temperatures ($T_M/2$) for instance, it is clear that a nonlinear athermal creep field separates the glide field from the Coble-creep field [21]. The temptation to include superplastic flow as an independent mechanism is great, but recent work [22,23] indicates that superplasticity is an accelerated form of diffusional flow. Twinning [24] and nonlinear grain-boundary sliding are ways of deforming a crystal although they cannot lead to unlimited deformation. Twinning is dominant at low temperatures, typically below 20°K and has, therefore, been ignored in the deformation maps for zirconium. Our present knowledge of these mechanisms is inadequate inasmuch as it cannot provide us with a viable constitutive equation - be it theoretical or empirical.

On the other hand, while studying the deformation properties of zirconium, it becomes clear that the metal behaves abnormally in particular ranges of stress and temperature. Several authors [1,19,20,21,25] have explained these abnormalities of zirconium

on the basis of models. In our present work we have attempted to include these mechanisms wherever possible. In general, the abnormal creep behavior of zirconium is attributed to:

i. High diffusion coefficient

ii. Low modulus of elasticity

iii. α (h.c.p.) $\rightleftarrows$ β (b.c.c.) phase transformation at slightly above $0.5T_M$

The next section discusses the peculiarities of zirconium in relation to the normally expected behavior of metals of the same class and crystal structure.

4. DEFORMATION OF ZIRCONIUM - THE PECULIARITIES

The variation of steady state creep rate over a wide range of stress for a typical metal polycrystal is shown in Figure 4-1 (Burke and Sherby [30]). The creep rate is normalized with respect to diffusion rate of the controlling atomic species. The figure depicts three basic regions, each region having a different relationship between steady state creep and the stress.

i. Low Stress Creep Range

Due to a stress directed atom-migration process, and generally referred to as diffusional creep. The behavior is typically valid at stresses below which $\dot{\varepsilon}/D$ equal to about 10^2.

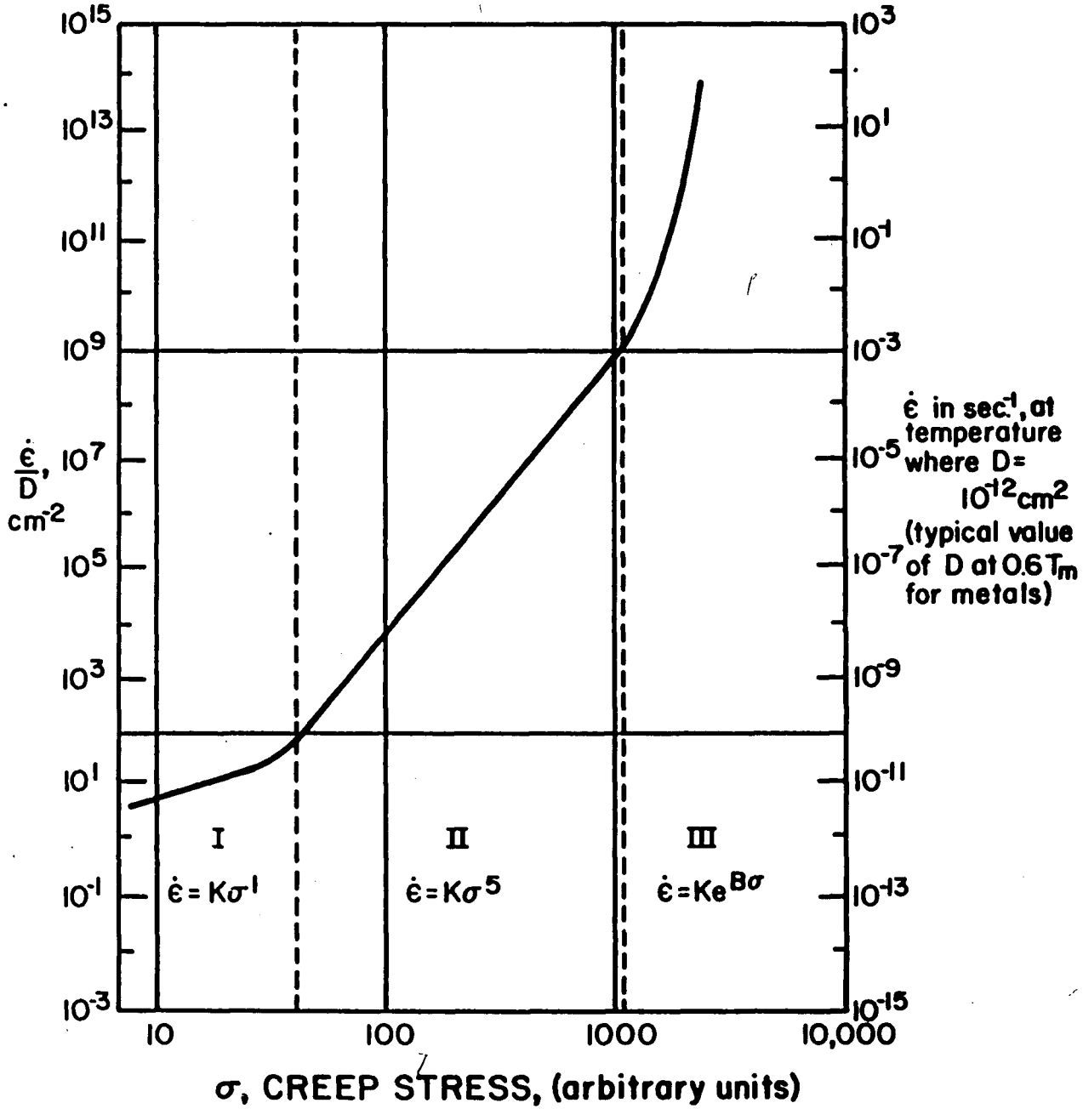

Fig.(4-1)- Variation of Steady State Creep Rate over a Wide Range of Stress for a typical metal polycrystal. Burke and Sherby [30]

ii. *The Intermediate Creep Range*

Believed to be controlled by either dislocation climb or by the non-conservative motion of jogs in screw dislocations. Most studies (Weertman [12], Barrett and Sherby [26] and Dorn [27]) indicate that the creep rate in this range is proportional to the diffusion coefficient and is a function of elastic modulus and stacking fault energy. This law, where

$$\dot{\varepsilon} = K\sigma^n \tag{4.1}$$

is typically valid between $10^2 < \dot{\varepsilon}/D < 10^9$, the value of 'n' (the stress exponent) for pure metals is usually observed to be around 5.

iii. *High Stress Creep Range*

Two theories of creep (Weertman [28] and Barrett and Nix [29]) associate high stress creep with the presence of a high vacancy concentration. Both theories deal with dislocation as sources and sinks for vacancies. The general equation proposed is:

$$\dot{\varepsilon} = K \exp(\beta\sigma) \tag{4.2}$$

Other mechanisms, as well as empirical relations have been proposed. For instance, Garofalo [31] has proposed an equation of the form

$$\dot{\varepsilon} = K (\sinh B\sigma)^n \tag{4.3}$$

Burke and Sherby [30] have made a comparative study of the various creep equations with the experimental data for high purity aluminum. The best correlation they observed has been with the Weertman equation for $T > 0.5T_M$ [2,26,27,28,29,30,31]. Miller and Sherby [19] have shown that for $T > 0.5T_M$ a modified form of Garofalo's equation better fits the experimental data. High stress creep typically occurs when creep rates are above $10^9 D$.

The above discussion on the steady state creep behavior demonstrated by most materials is to provide an analytical framework to compare the deviation of zirconium from typical polycrystalline metals.

a. "High Temperature" Creep of α-Zr

Ardell and Sherby [2] have shown that pure polycrystalline zirconium does not obey the creep-rate stress law depicted above. Its stress dependence is such that the exponent 'n' in the power law relation increases with decreasing stress (Figure 4-2, [2]). In order to explain this, Ardell and Sherby proposed a new controlling mechanism for creep of alpha-zirconium. In the Weertman [12] theory of creep it is envisioned that dislocations alternately glide and climb. In the light of what has been said earlier, these would be considered as sequential-dependent (parallel) processes and therefore the rate controlling process will be associated with the slower of the two. Weertman [12] herein makes an assumption

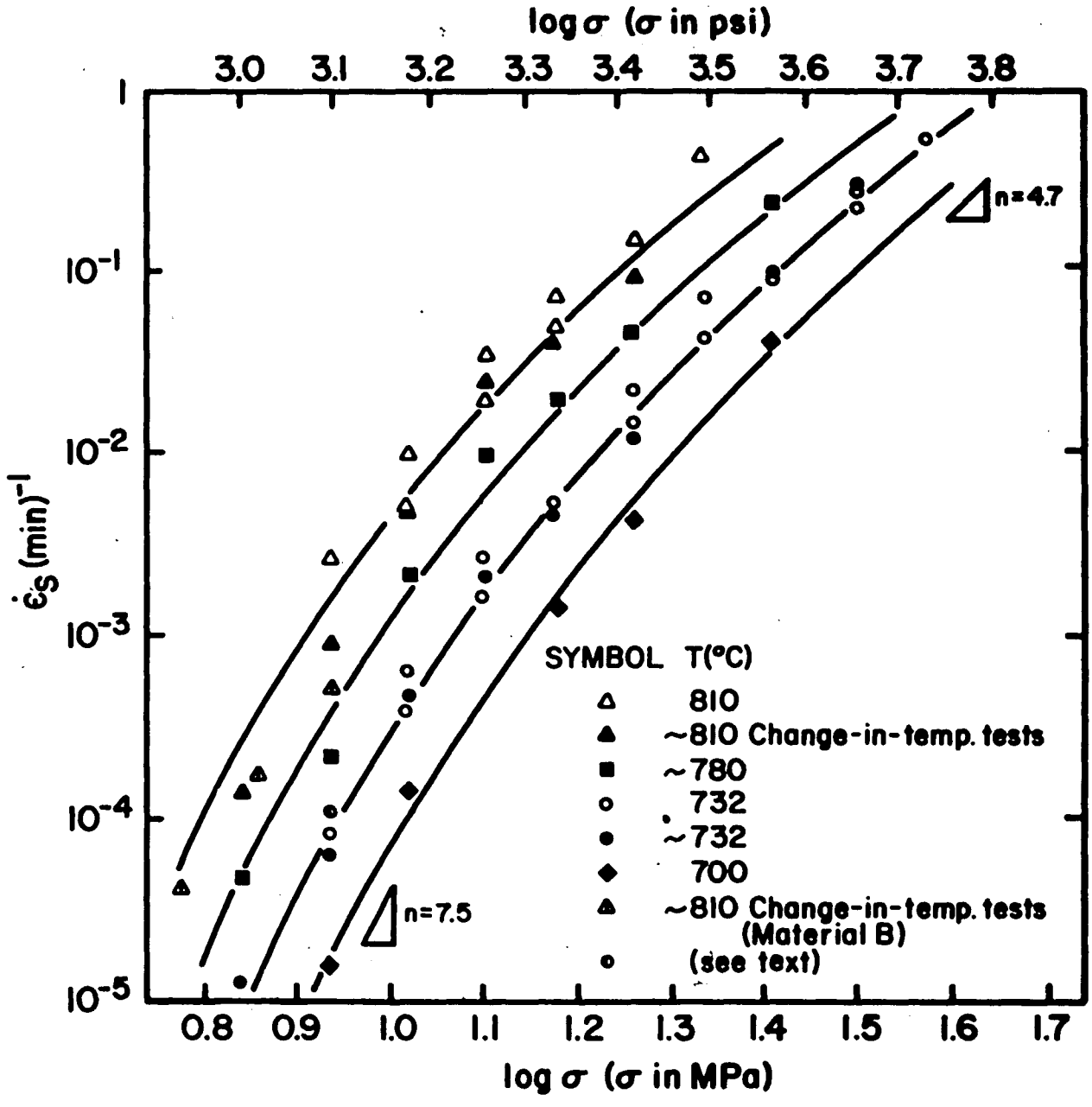

Fig.(4-2)-Steady state creep of alpha zirconium showing that the power law for creep is not obeyed for this material. Burke and Sherby

that dislocation climb is slower than dislocation glide, and derives a relation which explains the creep behavior of most pure metals. In the case of zirconium, however, the opposite is likely to be true, i.e. dislocation climb may be easier than dislocation glide at low stress levels due to:

i. High diffusion coefficient of alpha-zirconium ($D \simeq 10^{-12} cm^2/sec$ at $0.5T_M$ as compared to 10^{-16} cm^2/sec for most h.c.p. metals).

ii. Low elastic modulus ($= 4.8 \times 10^{11}$ dynes/cm^2 at $0.5T_M$).

Both high diffusivity and low elastic modulus lead to high climb rates. Thus the unusual creep behavior of alpha-zirconium may be due to a glide controlled creep process. Ardell and Sherby [2] have derived an equation using Gilman's [32] phenomenological equation relating dislocation velocity to the shear stress for the case where dislocation mobility is limited by the nucleation of kink motion:

$$\dot{\varepsilon} = C \exp(\beta\sigma)\exp\{-(Q_K + \eta/\sigma)/RT\} \qquad (4.4)$$

where

C, β, and η are constants

and Q_K = kink formation activation energy.

They considered two interpretations of their data, each requiring different values of the parameters β, C and n:

i. (*Model I*). The parameters are adjusted such that the equation above describes the data over the entire range of stress and temperature, implying that creep is controlled exclusively by dislocation glide ("Exclusive Glide Control").

ii. (*Model II*). The parameters are adjusted to allow for the possibility that at high stresses, the steady state creep of alpha-zirconium is diffusion-controlled whereas at low stresses the steady state creep rate is glide controlled. Here the postulation is that climb and glide are sequential processes, wherein the slower of the two is rate controlling ("Mixed Glide and Diffusion Control").

Knorr and Notis [1] have developed a deformation mechanism map of alpha-zirconium incorporating the "Mixed Glide and Diffusion Control" approach. During the course of this present study a similar map has been developed incorporating the "Exclusive Glide Control" approach. Experimental data was then superimposed on both the maps. Although both maps showed values that are within the limits allowed by experimental error, the "Mixed Diffusion and Glide" approach proved to be a better fit. A plausible explanation

for the above is the fact that if the temperature is greater than 0.5 T_M (or 0.5 T_α, where T_α is the $\alpha \rightarrow \beta$ phase transformation temperature) and the stress is high enough, the number of operative slip systems in the case of h.c.p. metals increases, so that glide becomes an easier process than climb. Another way of looking at this problem is to observe that, as stress is increased, the value of 'n' approaches 5.0 from 7.4 (Figure 4-2), leading to (or requiring) lower climb rates.

Thus above a certain stress level, glide controlled creep becomes faster than diffusion controlled creep and glide is no longer rate controlling, whereas at low stresses the reverse is true.

b. The Intermediate Temperature Region (375°C to 625°C)

The flow behavior of alpha-zirconium has been investigated in considerable detail at low temperatures (Tyson et al. [33], Sastry et al. [34]) and at high temperatures, (Bernstein [35], Ardell and Sherby [2]); however, the intermediate temperature region that includes the operating range of many zirconium based nuclear reactors lacks detailed investigation. Heritier et al. [3] and Miller and Sherby [4] have attempted to study this region. Both have put forth an explanation on the basis of phenomenology.

Heritier et al. [3] studied the deformation of alpha-zirconium between 375°C and 625°C and at strain rates from 5.0×10^{-6} to 10^{-1}

per second by compression testing. In this range of temperature and strain rate, they were able to distinguish three types of flow behavior:

i. At low temperatures and high strain rates, the yield stress was almost independent of temperature (Figure 4-3) and appeared to be relatively insensitive to strain rate (Figure 4-4).

The relative constancy of σ_y/E_o (where σ_y is the uniaxial yield stress and E_o the Young's Modulus) in the low temperature region suggests that the deformation mechanism controlling flow is an athermal one. The explanation put forth for this is that athermal creep is associated with the Orowan stress required to bow out segments of the Frank network, wherein the strengthening effect of solute addition is an indirect one, through the dislocation density and the mean segment length.

ii. At high temperatures and low strain rates the yield stress is observed to be strongly sensitive to temperature and strain rate. This behavior (also shown in Figures 4-3 and 4-4) is characteristic of overcoming a particular class of short-range obstacles by a thermal activation process. The mechanism proposed herein is node unpinning or a solute interaction mechanism.

iii. The transition region between low temperature athermal flow and high temperature "thermally activated" flow exhibits a "bell-shaped" upward bulge in the yield stress/temperature (Figure

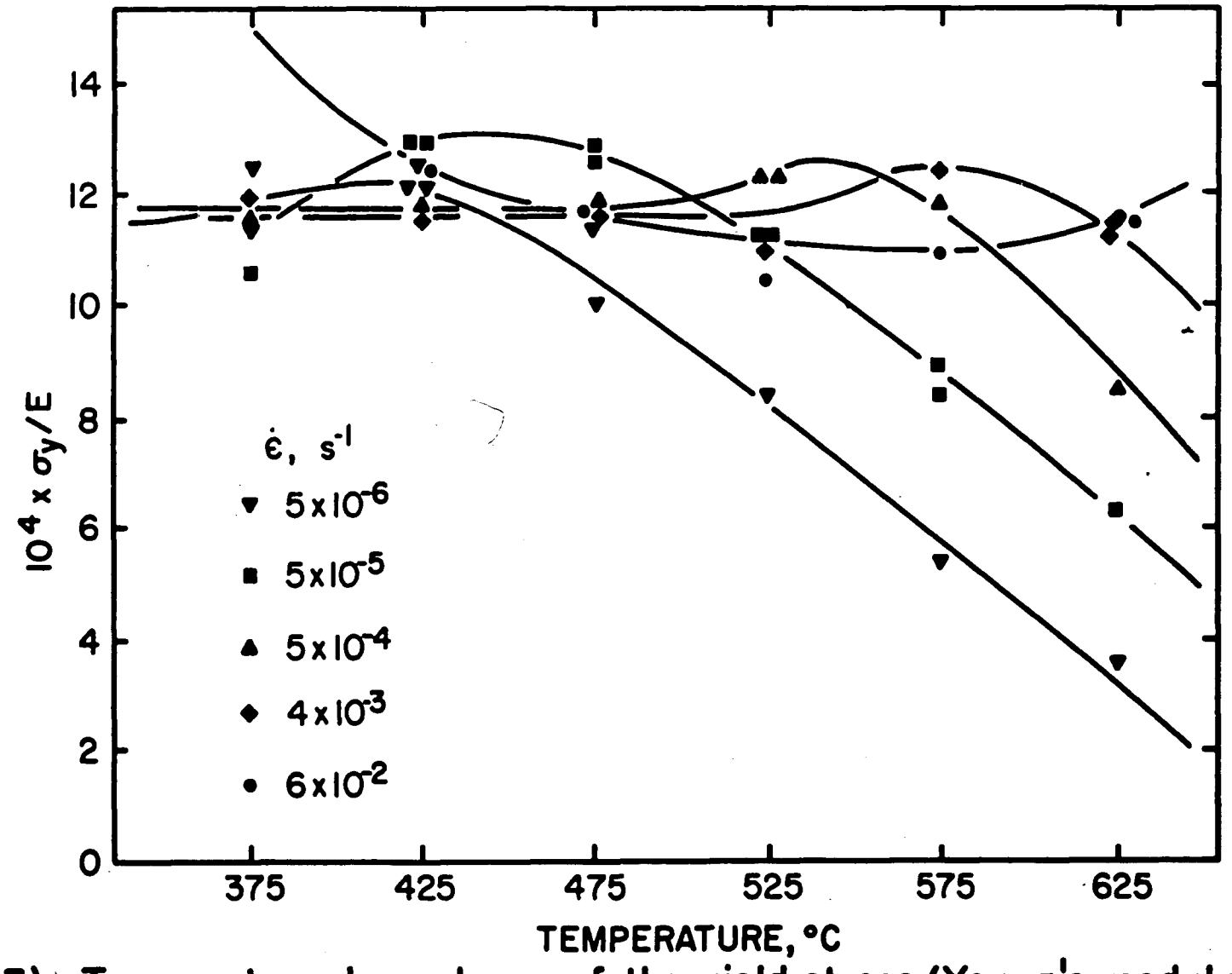

Fig.(4-3) - Temperature dependence of the yield stress/Young's modulus ratio. Heritier, Luton, and Jones [3]

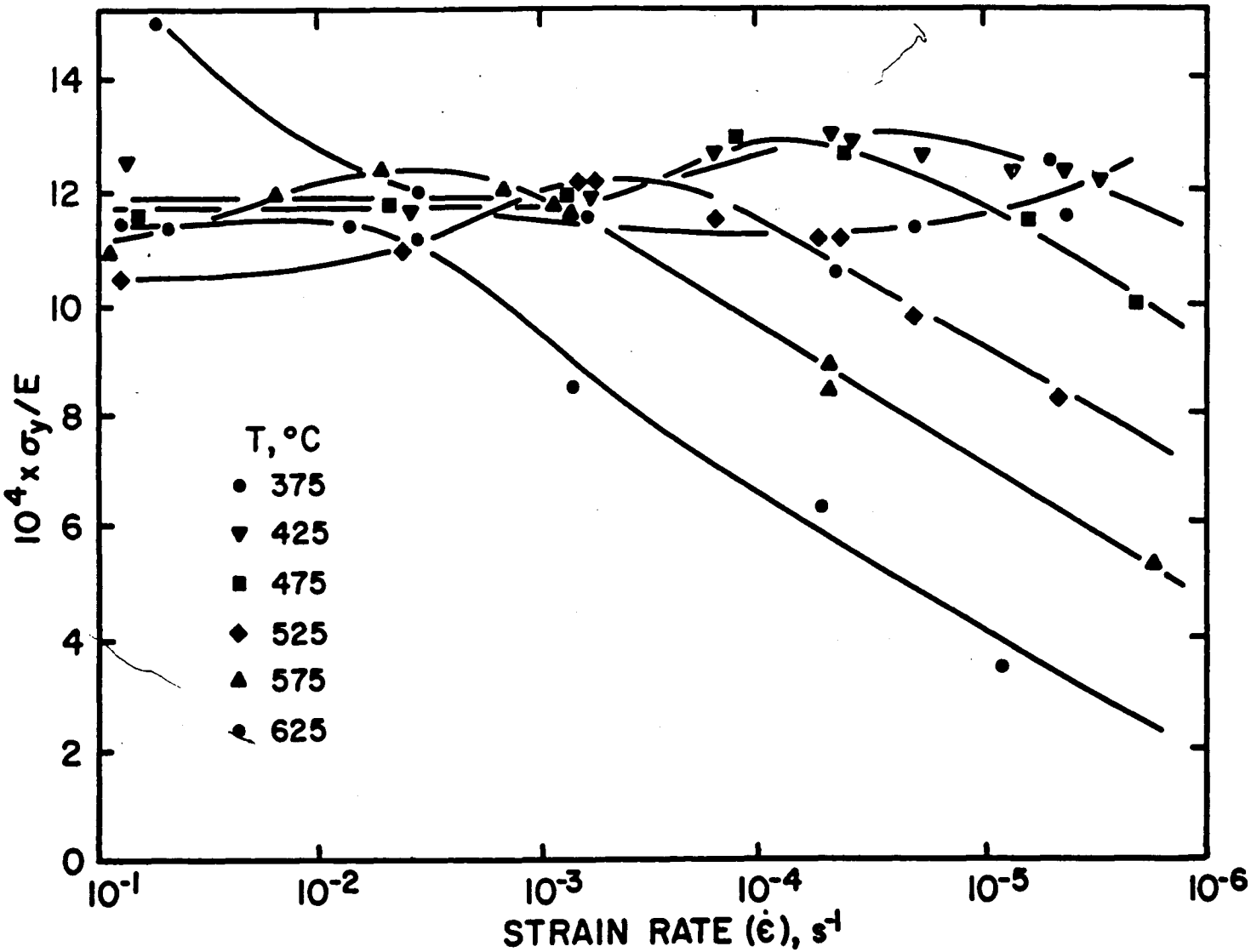

Fig.(4-4)- Strain-rate dependence of the yield stress/Young's modulus ratio. Heritier, Luton, and Jones [3]

4-3) and yield stress/strain rate plots (Figure 4-4). Also, as the strain rate is increased the "bell-shaped" region is displaced toward higher temperatures, although the width of the bell remains unchanged.

The authors [3] attribute this type of behavior, i.e., a flow stress increase in the transition region, to the presence of two separate flow components. First, there is a stress component arising from the transition from athermal to thermally activated flow in the absence of impurities; secondly, there is a stress component attributable to the presence of dynamic strain ageing. Finally, these flow stress maxima are typically found only in "commercially pure" alpha-zirconium, zirconium-oxygen and zirconium-nitrogen alloys [3]. A decrease in the impurity content has been observed to decrease, and even to suppress [3] the plateau and "bell-shaped" flow characteristics.

While the explanation presented by Heritier et al. to interpret the unusual behavior in the 375°C to 625°C range at first seems reasonable, a closer look reveals that their approach lacks a "single model" that can explain the abnormalities of alpha-zirconium in this temperature range. Miller and Sherby [4] have attempted to present a "single model" approach, although their work is not yet able to completely explain all aspects of the behavior of alpha-zirconium.

As opposed to the athermal creep approach of Heritier et al.

[3], Miller and Sherby [4] have tried to physically explain the observed behavior of zirconium in terms of the drag stress exerted by solute atoms on moving dislocations as proposed by Cotrell [36]. This drag stress is relatively small at either low or high temperatures, but over some intermediate temperature regime, the speed at which solute atoms diffuse is of the same order of magnitude as the dislocation velocities, and a higher drag stress can be exerted. The temperature regime for strong solute drag also depends on the strain rate. Thus the "plateau" in the yield strength versus temperature curve (Figure 4-3) can be adequately explained and modeled by a completely thermally-activated approach, i.e., without recourse to the athermal plastic flow mechanism suggested by the previous investigators.

Miller and Sherby [4] express the strain rate in terms of two stress components as follows:

$$\dot{\varepsilon} = B\theta' \left\{\sinh\left[\left(\frac{\sigma}{\sqrt{F_{sol}} + \sqrt{F_{def}}}\right)^{1.5}\right]\right\}^{n} \qquad (4.5)$$

where

F_{sol} = stress exerted by the solute atom on moving dislocations

F_{def} = history dependent stress created by deformation of the material

θ' = temperature-dependent term proportional to $\exp(-Q_R/RT)$

Q_R = activation energy for recovery, a function of current stress and current level of work hardening, F_{def}

B,n = constants.

The stress function related to solute strengthening, F_{sol}, as a function of temperature compensated strain-rate ($\dot{\varepsilon}/\theta' = Z$) is shown as the solid curve in Figure 4-5. The values of F_{sol} were calculated by Miller and Sherby from a fit to yield strength data [4]. The peaks shown in Figure 4-5 correspond to the solute species present in the material. These peaks are in fact analogous to the "bell-shaped" bulges described by Heritier et al. [3]. In Figure 4-6 the curve derived from the simulated model based on equation (4.5) is compared to the data available in the literature [4]. As it now stands, there is reasonable agreement for the 0.2 percent yield strength predictions and the steady state flow stress predictions as a function of temperature (Figure 4-6) but Miller and Sherby [4] report that the simulation underpredicts the room temperature flow stress by an uncomfortable margin. However, the part of the model (F_{sol}) that is responsible for simulating the sudden decrease in creep rate (Figure 4-7) is the same part of the model that is responsible for simulating the "plateau" in the yield strength versus temperature curve (Figure 4-6). The success in simulating this unusual decrease in creep rate can be interpreted as a verification of the modeling approach.

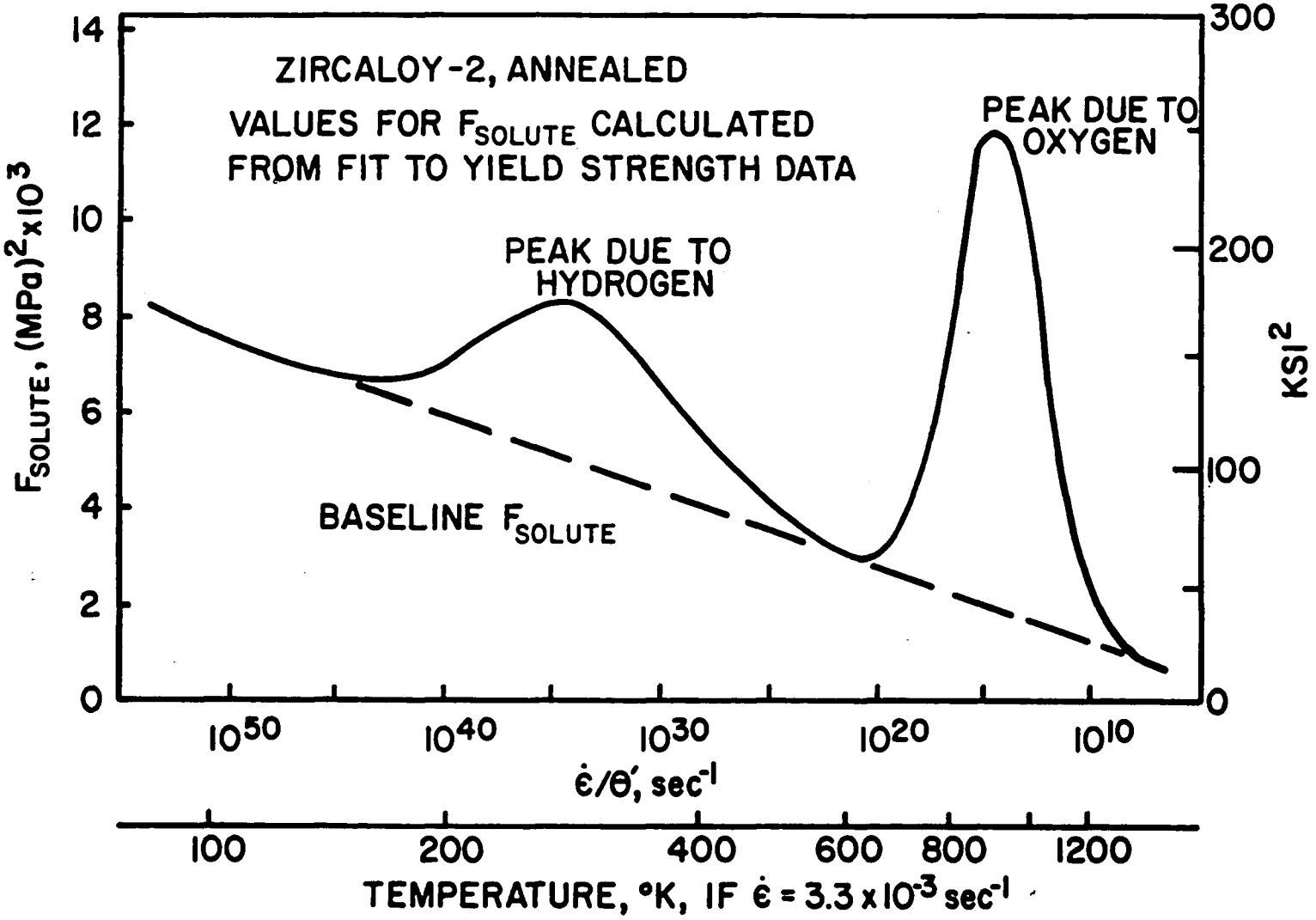

FIG.(4-5)- The solute strengthening term, $F_{sol.}$, as a function of temperature compensated $\dot{\epsilon}/\theta$. The line shown is the analytic fit described by the material constants, which were calculated from a fit to the yield strength data shown in Fig.(4-6). Miller and Sherby [4]

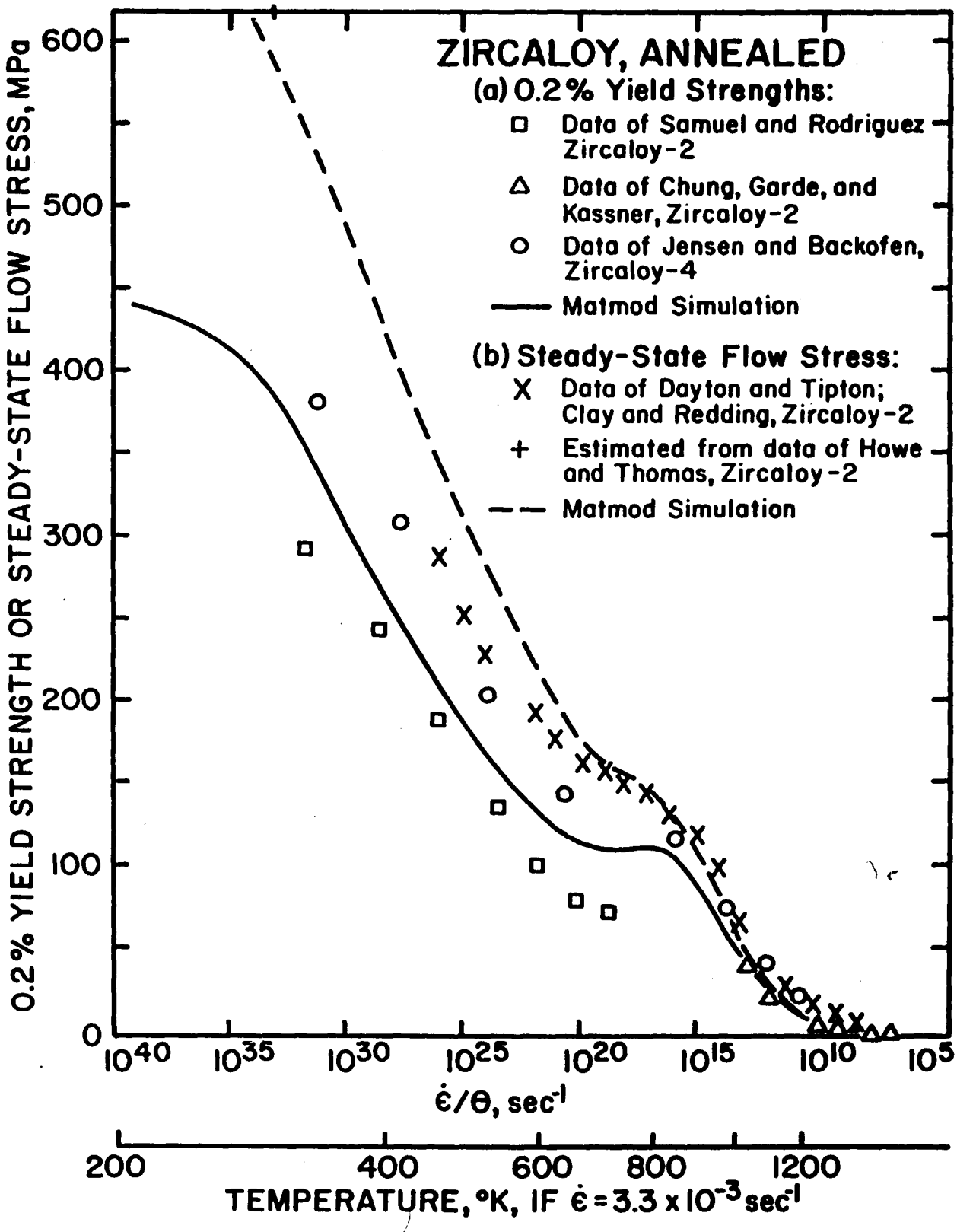

Fig.(4-6)- Simulated behavior of alpha Zirconium. Miller and Sherby [4]

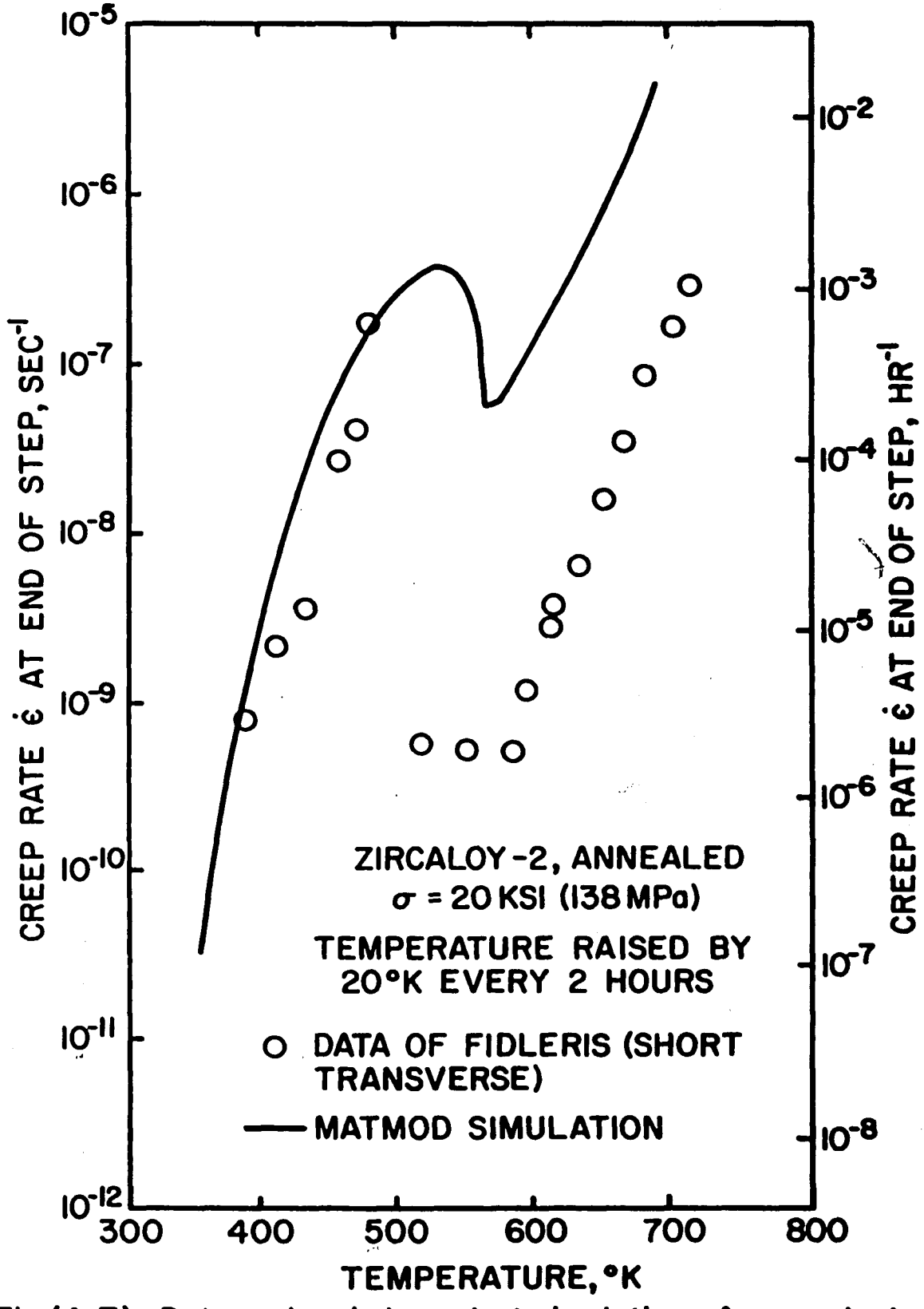

Fig.(4-7)- Data and an independent simulation of a constant stress, stepped temperature creep test. Both the data and simulation show a sudden decrease in creep rate which is associated with a sudden strong increase in Cottrell atmosphere solute effects.

It should be noted that this is the only constitutive equation that pays any attention to recovery, although it is known that stress present during recovery has a profound effect on the rate of deformation [4]. Hence the fact that one can make meaningful predictions incorporating a recovery term into the equation is important. As it now stands, the model is trying to physically explain observed behavior through a process of mathematical simulation; it therefore lacks identifiable material constants. As the model develops, and better constants are available, through better data, this problem may be resolved.

5. DEFORMATION MECHANISM MAPS

The interactive, complex behavior of the various creep deformation mechanisms that have been discussed in the previous sections can be presented on a map with axes of stress and temperature as shown by Frost and Ashby [5]. The map, Figure 5-1, is divided into fields which indicate regions of stress and temperature where each of the various mechanisms are dominant. Superimposed on the fields are contours of constant strain-rate that a given combination of stress and temperature will produce. Thus the map depicts the relationship between stress, temperature, and strain-rate. If two of the variables are known, the third can be obtained from the map. It can be seen that if the axes were strain-rate and stress, one could obtain constant temperature contours which could prove to be useful for isothermal tests. Also, if the axes were strain-rate

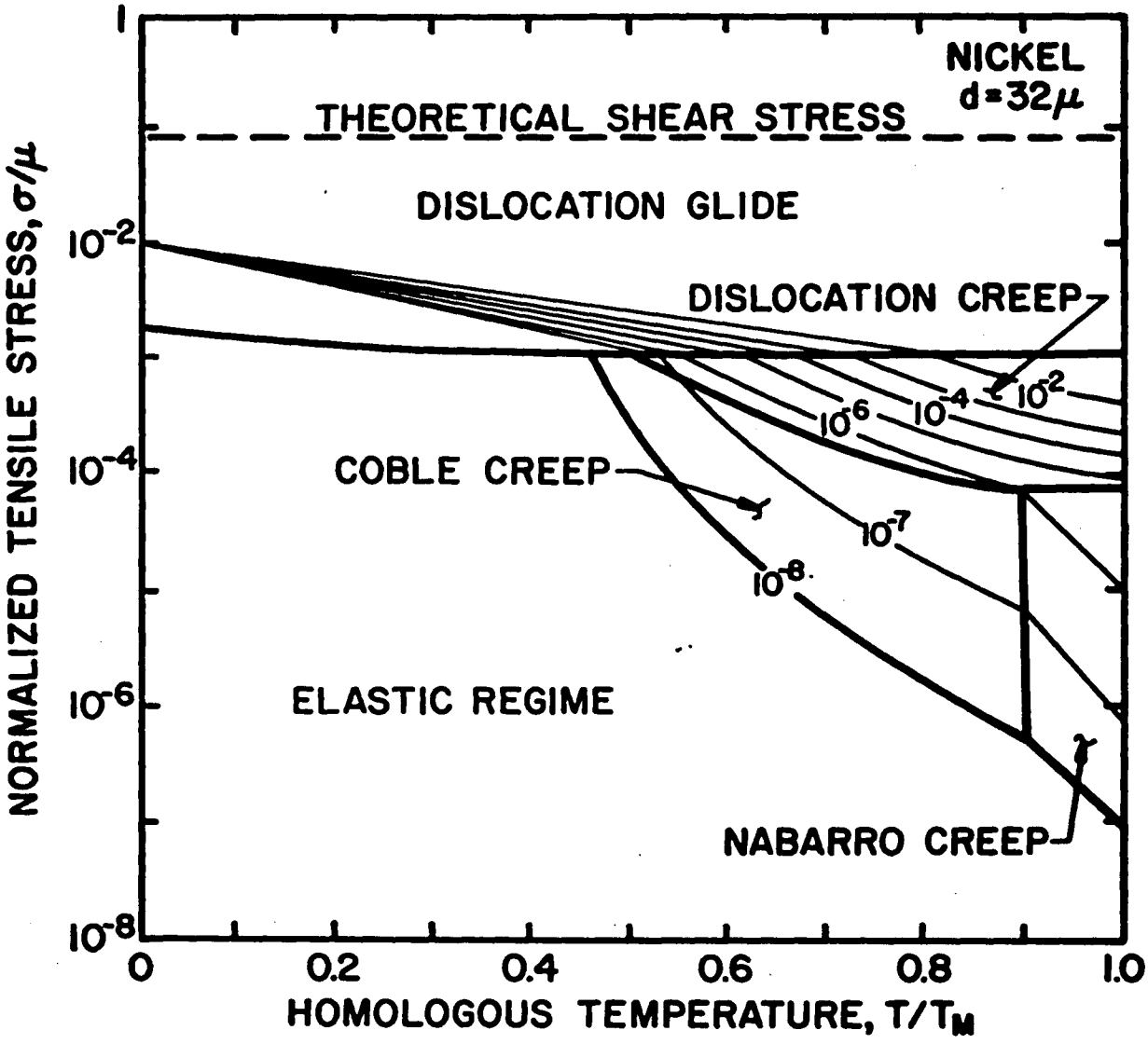

Fig.(5-1)-A typical Deformation Mechanism Map for Nickel (d=32μ). Elastic boundary = 10^{-8} sec^{-1} (Notis, after Frost and Ashby)

and temperature, constant stress contours could be obtained. These may be used for comparison of tests at constant stress. A third variation of this form has been developed by Smoak and Notis [42], and Mohamed and Langdon [43], who have introduced a deformation mechanism map based on plots of stress versus grain size with the temperature being constant.

All of these maps are constructed from rate-equations. The selection of the proper rate-equation should be based on the soundness of the physical model that the equation portrays. It should not be imprecise or too broad to predict exact values. Most often, theory gives the form of the equation, and experimental data helps evaluate the constants that enter the equation. The advantages of this phenomenology is that:

1. It can handle complicated phenomena more accurately.
2. It can be used to extrapolate outside the range for which data is available, while a purely empirical equation cannot.

The accuracy of the deformation maps depend on the validity of the assumptions made and the soundness of the model used. For example, the internal structure of a material that undergoes a martensitic transformation is bound to change with respect to dislocation density; also, atomic volume and Burger's vector will increase with an increase in temperature. However, these parameters

are usually taken as constant. According to Frost and Ashby [5] the inherent inaccuracy of the maps $\pm$ 10 percent for a given stress level. It may be higher for the strain-rate and temperature terms.

A deformation mechanism map for zirconium could prove to be quite useful to a design or maintenance engineer. For a given set of operating conditions he would be better able to evaluate the utility of the component and then reduce his conservatism in safety calculations. In general, the maps are useful in a qualitative way for choosing a material for applications, for predicting the mechanism by which it deforms and hence in selecting or predicting the effects of strengthening mechanisms. To a scientist, they help in providing insight and help in the designing of experiments to study a given flow mechanism, and in locating, identifying, and characterizing missing mechanisms.

The actual construction of the maps is done by a computer program which searches incrementally over the stress-temperature field to find the strain-rate contours and field boundaries. The program is relatively simple, consisting of a search algorithm and a plotting routine. The calculations are done primarily within a DO-loop that evaluates the rate-equation for a prescribed set of stress and temperature value. Also, it forms a sum of the contributions to the overall strain rate by each of the participating mechanisms and also solves for stress as a function of temperature at a constant strain-rate. The algorithm used provides for easy changes in rate equa-

tions or their form of interaction. The plotting routine is extremely flexible, and changes in the axes of the maps (say log $\dot{\varepsilon}$ vs log (σ/μ)) can be made without much difficulty.

In constructing the deformation maps, climb-controlled creep and diffusional flow are taken as independent mechanisms involving different defects. Therefore their strain-rates add. On the other hand, climb creep and glide involve the same defect (dislocations), although they describe different behavior patterns; the overall contribution of these two mechanisms is such that the slowest of the two processes controls deformation as outlined in the first section of this thesis.

In summary, the overall (net) strain rate of a polycrystal subjected to a stress 'σ' at a temperature 'T' is:

$$\dot{\varepsilon}_{net} = \dot{\varepsilon}_{ideal} + \dot{\varepsilon}_{diffusion} + \text{slowest of } (\dot{\varepsilon}_{glide}, \dot{\varepsilon}_{climb}) \quad (5.1)$$

In relation to the deformation map shown in Figure 5-1, within a field one creep contribution is larger than any other. The field boundary defines the values of 'σ' and 'T' at which a switch of dominant mechanism occurs. The contours of constant strain-rate are obtained by solving the above equation for 'σ' as a function of 'T' at constant $\dot{\varepsilon}$.

One of the major difficulties encountered in developing deformation mechanism maps for zirconium was the inclusion of the $\alpha \rightarrow \beta$ phase transformation at 862°C. Hence the deformation maps for

α-zirconium (upto 862°C) have been computed with constants found in the literature. Above 862°C and upto the melting point, β-zirconium constants have been used to compute a deformation map for β-zirconium. The two maps have then, been put together manually in order to obtain one deformation map for both α and β zirconium including the transformation.

According to the equilibrium phase diagram for the Zr-Sn system [45] the α→β transformation temperature is influenced only slightly by small Sn additions and it is not until about 5 wt percent Sn that a visible (α+β) two phase region appears [45]. However, it is observed that the (α+β) two phase region appears to widen when ternary additives are made (i.e., in zircaloy-4) and especially in the presence of an oxygen ambient atmosphere [46]. A broad two phase region could complicate the modeling of the deformation processes because of the introduction of a superplastic flow contribution related to the stable two-phase structure [46]. Again, for the purpose of simplifying our deformation maps and since our work refers to steady state creep in a vacuum or argon environment, we have chosen to use the same α→β transformation temperature for zircaloy-2 as for pure zirconium and we have also ignored the presence of a narrow two-phase region.

The specific values for constants used to compute the deformation mechanism maps have been chosen from available literature wherever possible. Some of these are empirically derived

to fit the spread permitted by experimental data. In certain cases, the values are derived by extrapolation of data and in still others values have been assumed based on materials that belong to the same group, e.g. titanium.

In the following section specific choice of values for each equation used in the computation for the maps are discussed.

For equation (4.4) namely:

$$\dot{\varepsilon}_s = C_{exp}(\beta\sigma)\exp\{-(Q_K + \eta/\sigma)/RT\}$$

the values are taken directly from Ardell and Sherby [2]. In Model I (Exclusive Glide Control) the parameters (C, β, Q_K and η) are adjusted so that the above equation describes the experimental data over the entire range of stress and temperature, implying that creep is controlled exclusively by dislocation glide. In Model II, the same parameters are adjusted to allow for the possibility that creep is diffusion-controlled at high stresses but glide-controlled at low stresses. In our computation we have assumed that β-zirconium creeps like a normal b.c.c. material, and since equation (4.4) was empirically derived specifically for α-zirconium, its application for β-zirconium does not arise. The values chosen are listed in Tables 5.1 and 5.2.

For the semi-empirical dislocation climb equation (3.3) namely:

$$\dot{\varepsilon} = \frac{A\, D_V\, b}{KT}\left(\frac{\sigma}{\mu}\right)^n$$

Table 5.1 Creep equation parameters for zirconium

Alpha-Zirconium

Parameter	Model I	Model II	Reference
$C(sec)^{-1}$	1.05×10^{9}	2.5×10^{7}	[2]
$\beta(dyne/cm^2)^{-1}$	3.1×10^{-9}	1.7×10^{-8}	[2]
Q_K(cal/mole)	50,000	50,000	[2]
η(cal dyne/cm^2)	1.75×10^{12}	1.27×10^{12}	[2]
A	N.A.*	1.85×10^{7}	[2]
n	N.A.*	4.70	[2]
D_ℓ^o(cm /sec)	5.9×10^{-2}		[47]
Q_ℓ(cal/mole)	52,000		[47]
$\mu(dyne/cm^2)$	[3.4 x 10" -	$2.36 \times 10^{8} T(°C)$]	[1]
b(cm)	3.226×10^{-8}		[1]
$\Omega(cm^3)$	2.32×10^{-23}		[35]
W(cm)	10^{-7}		[35]
$D_{gb}^o(cm^2/sec)$	0.75		[35]
Q_{gb}(cal/mole)	26,700		[35]
$\dot{\varepsilon}_p(sec)^{-1}$	10"		[5]
p	0.75		[5]
q	1.33		[5]
τ_p(dyne/cm)	0.2μ		*1
ΔF_K(ergs)	$0.2\mu b^3$		*2
$\dot{\varepsilon}_o(sec)^{-1}$	1.0×10^{6}		[5]

*Model I involves "Exclusive Glide Control" and therefore the dislocation climb equation (3.2) does not enter the picture.

Table 5.1 (Continued)

Parameter	Model I	Model II	Reference
τ_o(dynes/cm^2)	$\mu b\sqrt{\rho}$		*3
ρ(lines/cm^2)	6.25×10^8		*4
ΔF(ergs)	$0.2\mu b^3$		*5
Beta-Zirconium			
n	4.2		*6
A	6.03×10^3		[11]
$D_\ell^o(1)$(cm^2/sec)	1.34		[14]
$Q_\ell(1)$(cal/mole)	6.52×10^4		[14]
$D_\ell^o(2)$(cm^2/sec)	8.5×10^{-5}		[14]
$Q_\ell(2)$(cal/mole)	2.77×10^4		[14]
μ(T)(862°C) (dynes/cm^2)	$[3.38 \times 10^{11} - 4.1 \times 10^8(T)]$		*7
μ(after 1200°C)	1.96×10^{11}		*7
b(cm)	6.26×10^{-8}		[49]
Ω(cm^3)	4.7×10^{-23}		[49]
W(cm)	1.0×10^{-7}		[35]
D_{gb}^o(cm^2/sec)	1.34		[23]
Q_{gb}^o(cal/mole)	3.91×10^4		[23]
$\dot{\varepsilon}_p$(sec^{-1})	10^{11}		[5]
p	0.75		[5]
q	1.33		[5]
τ_p(dynes/cm^2)	0.1μ		*1

Table 5.1 (Continued)

Parameter	Model I	Model II	Reference
ΔF_K(ergs)	$0.1 \times \mu b^3$		*2
$\dot{\varepsilon}_o(sec)^{-1}$	1.0×10^6		[5]
ΔF(ergs)	$0.1 \times \mu b^3$		*5
T_o(dynes/cm^2)	$\mu b\sqrt{\rho}$		*3
ρ(lines/cm^2)	6.25×10^8		*4

Table 5.2 Creep equation parameters for Zircaloy-2

Alpha-Region

Parameter	Model I	Model II	Reference
$C(sec)^{-1}$	3.5×10^{6}	2.88×10^{4}	*8
$\beta(dyne/cm^2)^{-1}$	1.1×10^{-9}	1.20×10^{-8}	*8
$Q_K(cal/mole)$	50,000	50,000	[2]
$\eta(cal\ dyne/cm^2)$	1.75×10^{12}	1.27×10^{12}	[2]
n	N.A.*	4.5	[2]
A	N.A.*	7.00×10^{5}	[11]
$D_\ell^o(cm^2/sec)$	12.6		[47]
$Q_\ell(cal/mole)$	64,300		[47]
$\mu(T)(dynes/cm^2)$	[3.4 x 10" -	$2.36 \times 10^{8} T(C°)$]	[1]
b(cm)	3.226×10^{-8}		[49]
$\Omega(cm^3)$	2.32×10^{-23}		[35]
W(cm)	10^{-7}		[35]
D_{gb}^o	17.5		[35]
Q_{gb}	42,500		[35]
$\dot{\varepsilon}_p(T)(sec^{-1})$	10"		[5]
p	0.75		[5]
q	1.33		[5]
$\tau_p(dynes/cm^2)$	0.2μ		*1
$\Delta F_K(ergs)$	$0.2\mu b^3$		*2
$\dot{\varepsilon}_o(sec)^{-1}$	10^{6}		[5]

*Model I involves "Exclusive Glide Control" and therefore the dislocation climb equation (3.2) does not enter the picture.

Table 5.2 (Continued)

Parameter	Model I	Model II	Reference
ΔF(ergs)	$0.2\mu b^3$		*5
T_o(dynes/cm^2)	$\mu b\sqrt{\rho}$		*3
ρ	6.25×10^8		*4
Beta-Region			
n	4.1		*9
A	4.01×10^4		[11]
$D_\ell^o(1)$(cm^2/sec)	1.34		[14]
$Q_\ell(1)$(cal/mole)	6.52×10^4		[14]
$D_\ell^o(2)$(cm /sec)	8.5×10^{-5}		[14]
$Q_\ell(2)$(cal/mole)	2.77×10^4		[14]
b(cm)	6.26×10^{-8}		[49]
Ω(cm^3)	4.7×10^{-23}		[49]
W(cm)	1.0×10^{-7}		[35]
D_{gb}^o(cm^2/sec)	1.34		[23]
Q_{gb}(cal/mole)	3.91×10^4		[23]
$\dot{\varepsilon}_p$(sec^{-1})	10"		[5]
p	0.75		[5]
q	1.33		[5]
T_p(dynes/cm^2)	0.1μ		*1
ΔF_K(ergs)	$0.1\mu b^3$		*2
$\dot{\varepsilon}_o$(sec^{-1})	10^6		[5]

Table 5.2 (Continued)

Parameter	Model I	Model II	Reference
ΔF(ergs)	$0.1\mu b^3$		*5
T_0(dynes/cm^2)	$\mu b\sqrt{\rho}$		*3
ρ(lines/cm^2)	6.25×10^8		*4

*1 Frost and Ashby [5] have shown that the value of T_p will differ by some appropriate Taylor factor depending on the crystal structure and slip systems involved. For h.c.p. metals it is 0.2μ and for b.c.c. metals it is 0.1μ. See Text.

*2 Frost and Ashby [5] have shown that ΔF_K directly reflects the nature and strength of the interatomic forces: these are to be determined by fitting equation (3.6) to experiment. However due to lack of available data values typical of h.c.p. metals ($0.2\mu b^3$) and b.c.c. metals ($0.1\mu b^3$) are chosen. See Text.

*3 The value of T_0 is the flow stress in the absence of thermal activation. Frost and Ashby [5] suggest noting the simplified form presented above.

*4 ρ specifies the degree of work-hardening. Zirconium is normally rolled before use and the value chosen corresponds to it.

*5 Frost and Ashby [5] have shown that the value of ΔF depends on the strength of the obstacles. A classification of the obstacles is given in the text. α-Zr is normally rolled and hence the value of ΔF chosen corresponds to that of obstacles such as forest dislocations whereas the value for β-Zr (b.c.c.) corresponds to that of isolated solute atoms and Peierls barriers.

*6 Values calculated from experimental data given in [22].

*7 A linear extrapolation of the shear modulus obtained from Koster [48] leads to negative values. Hence after 1200°C, a constant value of 1.96×10^{11} dynes/cm^2 has been used for the computation of the maps.

*8 Values calculated from experimental data given in [2].

*9 The value chosen corresponds to the value of β-titanium [56]. See Text.

The dimensional material parameters A and n have been taken from Ardell and Sherby [2] (see Figure 4-2) for α-zirconium. In the case of β-zirconium the value of 'n' has been taken from H. M. Chung et al. [22]. The corresponding value of A is then calculated from the following equation:

$$\log_{10} A = -10.5 + 3.4n \qquad (5.2)$$

as put forth by Stocker and Ashby [11].

The lattice diffusion constants for α-zirconium used in the above equation are interpreted from the data of Lyashenko et al. [47], whereas the diffusion constants for β-zirconium are taken from Kidson [14]. Kidson [14] has been able to explain the anomalous lattice diffusion of β-zirconium in terms of two lattice diffusion coefficients $D_\ell^o(1)$ and $D_\ell^o(2)$. The values are as listed in Tables 5.1 and 5.2. The total diffusion rate is then given as:

$$D = D_1 + D_2$$

The shear modulus and Burger's vector values in the case of α-zirconium are taken directly from Knorr and Notis [1]. The shear modulus for β-zirconium is shown to vary linearly with temperature by Koster [48]; but a linear extrapolation leads to negative values after 1200°C and hence a constant value of 1.96 x 10" dynes/cm^2 has been used for the computation of the maps beyond 1200°C. The Burger's vector value has been taken directly from the Reactor Handbook [49].

Values for the parameters in the Coble creep equation (3.2) namely: D_b and W, are experimental values taken from Bernstein [35] for α-zirconium and the α-region of zircaloy-2. For β-zirconium Kidson [14] has shown that $D_\ell^o(1)$ is associated with lattice diffusion. The values used for the grain boundary diffusion constants are assumed as follows:

$$Q_{gb} = 0.6Q_\ell^o(1)$$

$$D_{gb}^o = D_\ell^o(1)$$

For β-zircaloy, the values are assumed to be the same as for β-zirconium. The values of Ω and Burger's vector are obtained from the Reactor Handbook [49].

Finally, the values for the parameters in the high temperature dislocation glide equations (3.6) and (3.7) are taken from the work of Frost and Ashby [5]. The values chosen for α-zirconium are values typical of h.c.p. materials, whereas the values for β-zirconium are typical of b.c.c. materials.

Frost and Ashby [5] have shown that the value of τ_p, the flow stress at 0°K, in the rate equation (3.6) will differ by some appropriate Taylor factor ($\bar{M}$) between single crystals and polycrystalline samples. The proper value should depend on the crystal structure and slip systems involved. Various calculations of the Taylor factor [5] show that typical values of τ_p for b.c.c. metals is 0.1μ and 0.2μ for h.c.p. metals.

The atomic structure enters equation (3.6) via ΔF_K, Helmholtz free energy of an isolated pair of kinks, which directly reflects the nature and strength of the interatomic forces [5]. Ideally these are to be determined by fitting equation (3.6) to experimental values. However, due to a lack of available data, values typical of b.c.c. and h.c.p. materials have been chosen:

ΔF_K (for α-zirconium) = $0.2\mu b^3$

and

ΔF_K (for β-zirconium) = $0.1\mu b^3$

The values of T_o and ΔF in equation (3.7) are obtained from Frost and Ashby [5]. ΔF is the total free energy required to overcome the obstacle without aid from external stress. Frost and Ashby [5] have classed the obstacles as follows:

Obstacle Strength	ΔF	Example
Weak	$<0.2\mu b^3$	Isolated solute atoms; Peierls Barriers.
Medium	$\sim 0.2\mu b^3$	Forest dislocations; radiation damage.
Strong	$>\mu b^3$	Dispersions; most precipitates.

For h.c.p. α-Zr, since the material is normally cold worked, a value of $0.2\mu b^3$ has been chosen. In the case of b.c.c. β-zirconium a value of $0.1\mu b^3$ has been used in the computation of the maps.

The data for zircaloy-2 is more freely available from the literature as shown in Tables 5.1 and 5.2. The values chosen are typical of those available. The values of n and A in equation (3.3) for the β-zircaloy region are assumed to be the same as for β-zirconium. In addition the values for the material parameters C and β in equation (4.4) are obtained by back calculations from experimental data.

6. EXPERIMENTAL PROCEDURE

To prove (or disprove) the validity of a model, it is necessary to compare the experimental and theoretical values. The deformation maps may be used as a visual means to display this comparison. The experimental data is plotted on the same axes, and the parameters are adjusted in a logical manner until the map matches experiment (within the accuracy of the experiment). In the maps shown, most of the adjustments were made mainly with 'n' and 'A' in the dislocation climb equation. Also, the parameters in the obstacle-limited glide equation needed to be adjusted. All the available data is converted to tensile stress for plotting and comparison purposes.

Although there is a substantial amount of creep data for α-Zr in the literature, there is no data available for β-Zr (except for Chung, Garde and Kassner [22] who have recently generated data for zircaloy). It was therefore decided to perform creep experiments on pure β-Zr in order to test the validity of our maps.

Zirconium of 98.5 percent purity was obtained from Teledyne Wah Chang Company, Albany, Oregon, in the form of bars. A spectroscopic analysis of the sample provided by the supplier showed that it has the following composition (wt%):

Zr + Hf	>99.2
Zr	>98.5
Fe + Cr	0.10 max.
N	.003 max.
C	0.017 max.
Hf	0.009 max.

Material of a higher purity was not purchased, because the purer material tends to recrystallize (even after annealing) after a few percent strain [2].

Compression creep tests were performed under constant stress conditions using equipment previously described by Krishnamachari [50]. This apparatus is capable of achieving temperatures as high as 1200°C; the load was applied through a lever arm and the stress was estimated to vary by no more than 5 percent. The extension of the specimen during creep was measured by means of a Linear Variable Differential Transformer (LVDT) with its movable core attached to the upper linkage of the stress application system. The output from the LVDT was rectified and fed by means of an electronic circuit that allowed the output to be placed conveniently on any of

the three ranges of an automatic recorder having an accuracy of ±1 percent. The specimen temperature was measured by means of a thermocouple placed close to the center of the specimen. The temperature was controlled to within ±1°C during the actual experiment.

The type of test procedure employed was one involving changes in stress at constant temperature. Due to the high oxidizing tendency of zirconium, the tests were conducted in an atmosphere of argon.

Chung, Garde, and Kassner [22] have shown that in contrast to the α-phase, the β-phase exhibits considerable grain growth which is not dependent on the oxygen concentration. The rapid grain growth in the β-phase can be attributed to the large diffusivity associated with the body-centered cubic lattice. At 1350°C the grains achieve a stable size in 15-20 minutes. This required heating the sample to a constant temperature approximately 100°C above the test temperature for about an hour, so that a stable grain size is obtained. The temperature is then lowered to the test temperature and the experiment conducted.

The specimens with excellent surface finish were prepared by using a diamond saw. Creep specimens were in the shape of upright rectangular prisms approximately 0.1" x 0.1" x 0.2" high. All the specimens were chemically etched prior to the annealing treatment to remove surface contamination. The etching solution consists

of 45 parts HNO_3, 30 parts H_2O, 15 parts H_2O_2 and 8 to 10 parts HF [2].

During the tests, the specimen was crept until the establishment of a well defined steady state, $\dot{\varepsilon}_1$ at σ_1, (which normally took about 20 minutes) whereupon the load was increased to a new value, $\dot{\varepsilon}_2$ at σ_2, and the test continued. The same procedure was followed for as many steady state rates as could be obtained from one specimen. The stress exponent, n, could be evaluated from the incremental stress tests using the expression:

$$n = d \log \dot{\varepsilon}/d \log\sigma \qquad (6.1)$$

This expression may be derived quite easily from the assumed relation $\dot{\varepsilon} = K\sigma^n$.

The specimens were prepared for metallographic examination in the usual manner. This consists of mounting the specimens in bakelite molds, followed by grinding through 4/o emery paper. This was followed by polishing down to Linde B, whereupon the specimens were chemically etched with the solution mentioned earlier. The grain size before and after the experiment was measured [51] to determine if there was any grain growth during the testing. A typical photomicrograph of the structure of a specimen after creep is shown in Figure 6-1. Values of grain size ranged from ~60μm for the as-received material and between 65-72μm after creep.

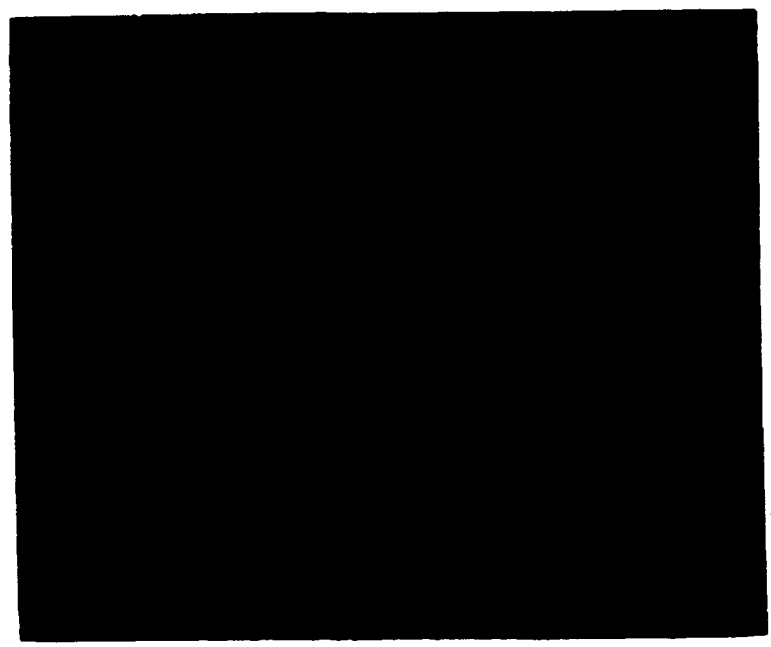

Fig.(6.1) - Typical Photomicrograph of Zirconium After Creep at 985°C. Average Grain Size = 68 μm. Note that the Increase in Grain Size from the As-received Material (≈60 μm) is Fairly Small.

The increase in grain size for the tested material is approximately 5 microns for a specimen having a grain size of 60 microns. This indicates that heating the specimen to 100°C above the test temperature, maintaining it at that temperature for 20-30 minutes, and then lowering the temperature to the test temperature is a suitable method for preventing an increase in grain size during creep testing. A tabulation of the experimental creep results is presented in Appendix I.

Measurements are made of the increments $\Delta\ell$ of elongation which are produced by successive additions of the total tensile load. The total true strain (ε) are obtained by using

$$\varepsilon = \ell n \left[\frac{L_o - \Delta\ell}{L_o}\right]$$

where

L_o = the original length of the test specimen

$\Delta\ell$ = the incremental decrease in length

The strain rate is then calculated by using the following formula:

$$\frac{\varepsilon_2 - \varepsilon_1}{t_2 - t_1} = \dot{\varepsilon}$$

where

ε_1 = the true strain observed at time t_1

ε_2 = the true strain observed at time t_2

7. DISCUSSION

Deformation maps for zirconium are plotted at three grain sizes, 10, 60, and 300 microns in Figures 7-1 to 7-3. These grain sizes were chosen because experimental data exists at these grain sizes to compare against computer-generated maps. These maps include regions for both α- and β-Zr as outlined in Section 5. A summary of the experimental data used is also presented in tabular form along with each figure.

In Figures 7-2A and 7-2B the experimental data of Bernstein [35] have been included. The number corresponding to each point is the logarithm of the experimentally observed creep rate. The experimental strain rates are in better agreement with the rates predicted on the map at each particular condition of stress and temperature for the "Mixed Glide plus Climb" model, than the "Exclusive Glide" model. A dominant Coble creep contribution is predicted at low stresses in the deformation map for this grain size (60 microns) and has been substantiated by Bernstein [35]. A dominant Coble creep regime is not observed for similar experimental stress conditions at a grain size of 300 microns.

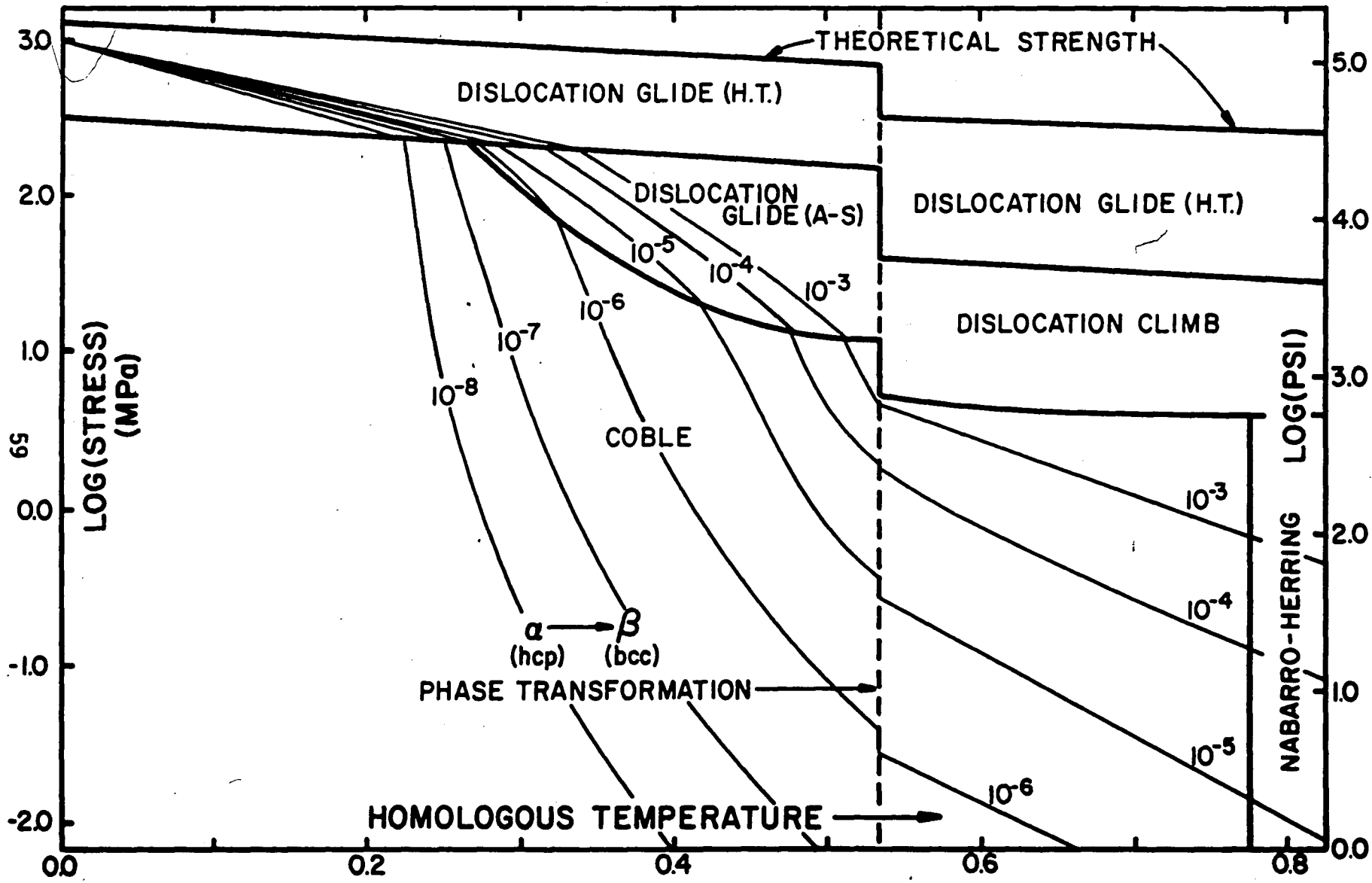

Fig.(7-1A)- Deformation Mechanism Map for Zirconium. Model I- Exclusive Glide Control. Grain Size = 10 microns

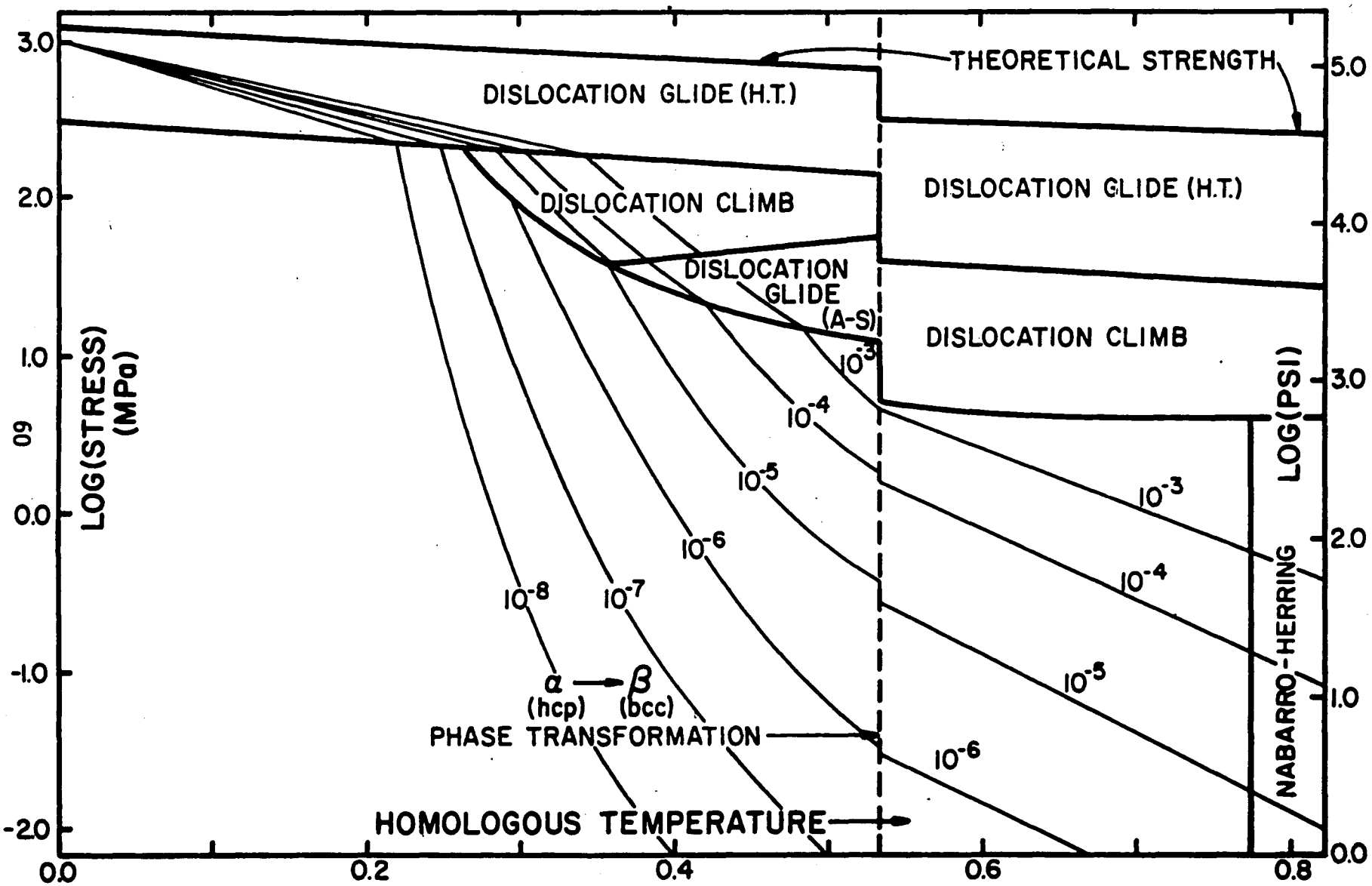

Fig(7-1B)- Deformation Mechanism Map for Zirconium. Model II - Mixed Glide and Climb Control. Grain Size = 10 microns

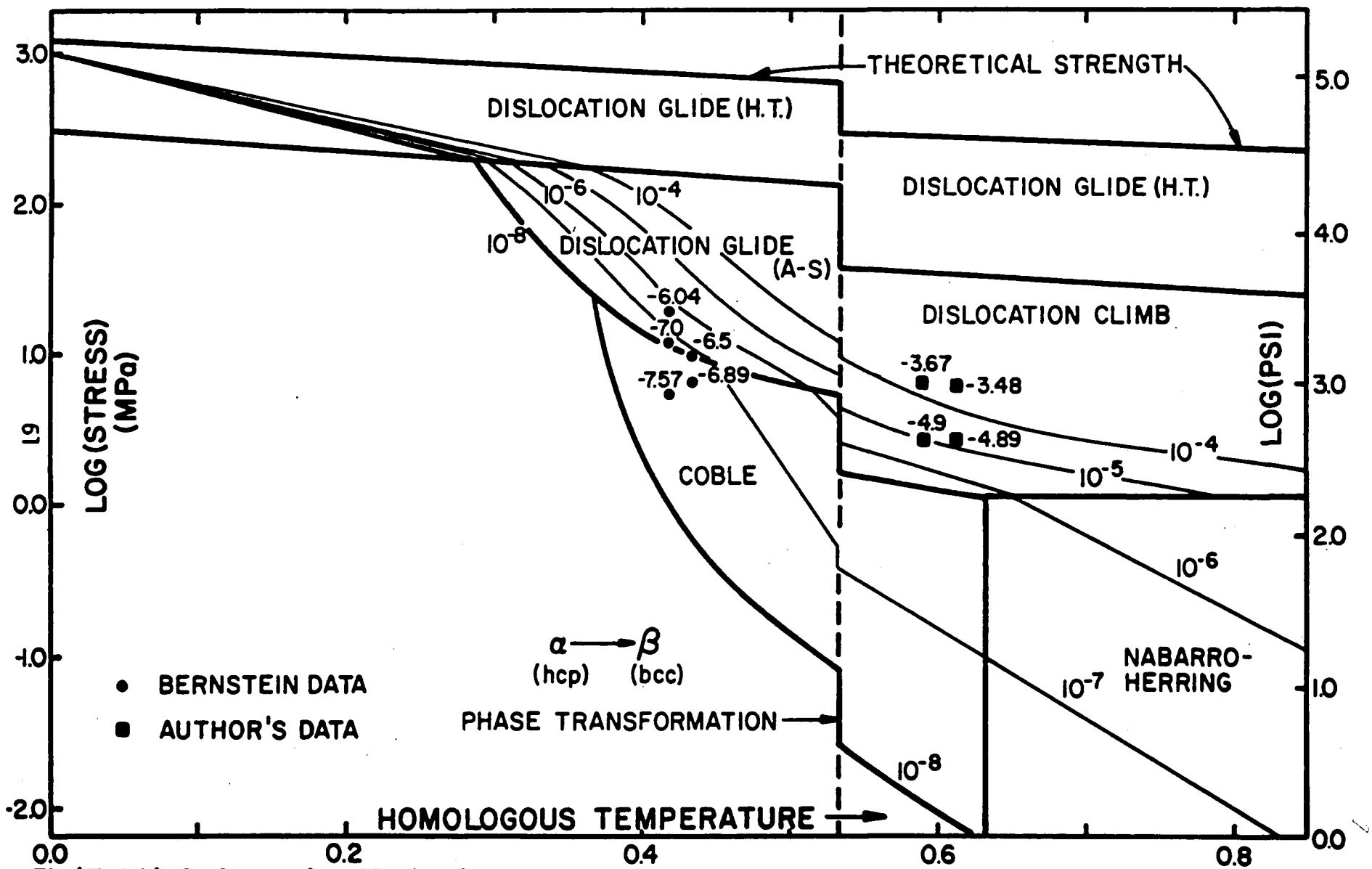

Fig(7-2A)- Deformation Mechanism Map for Zirconium. Model I - Exclusive Glide Control. Grain Size = 60 microns

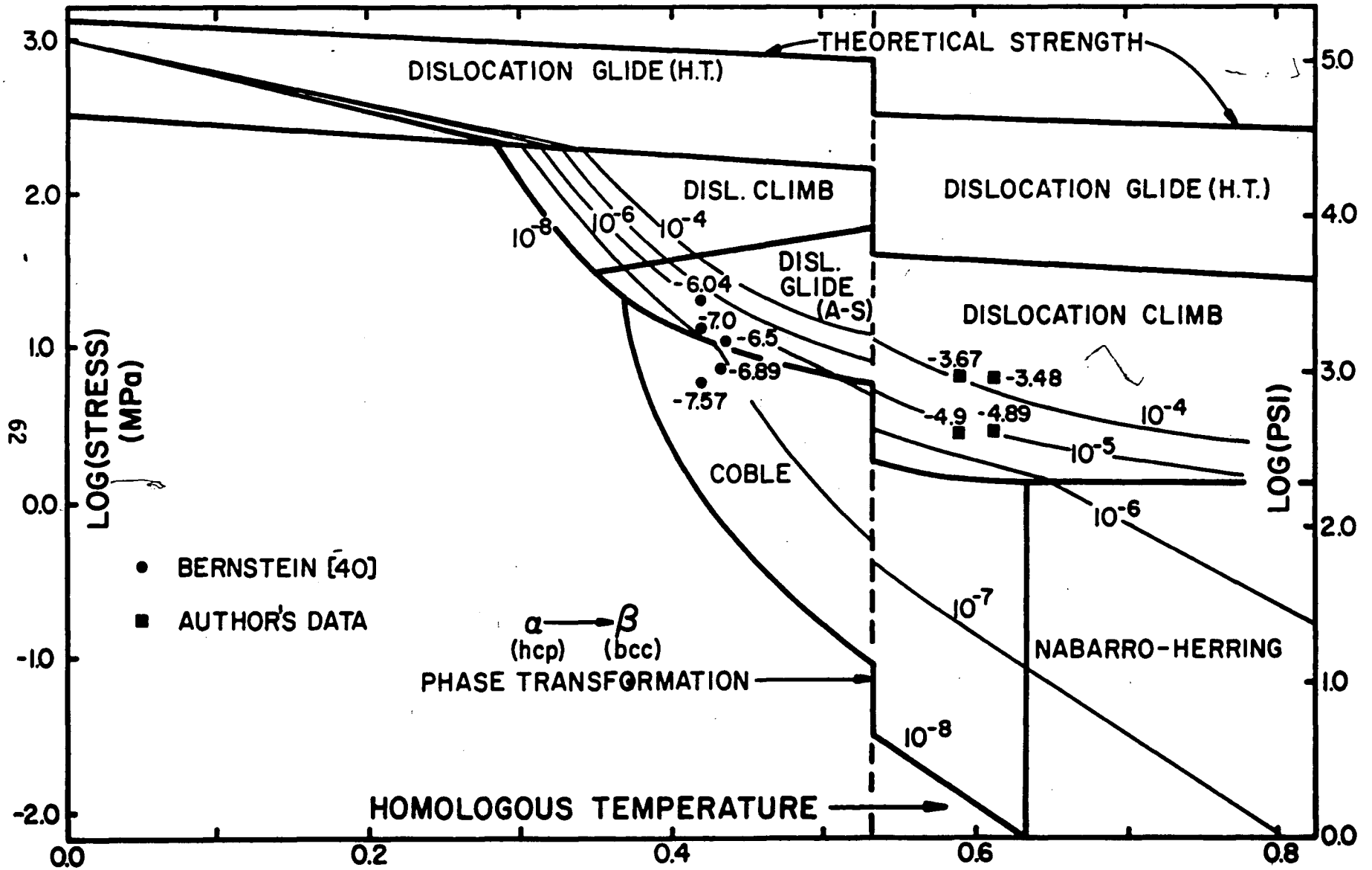

Fig.(7-2B)- Deformation Mechanism Map for Zirconium. Model II - Mixed Glide and Climb Control. Grain Size = 60 microns

Figure 7-2A and B. ALPHA-ZIRCONIUM
Experimental creep data at nominal
60 μm grain size

G.S. Microns	Homologous Temperature T/T_M	Log σ MPa	$\dot{\varepsilon}(Sec^{-1})$	Log $\dot{\varepsilon}$	Ref.
59	0.415	0.838	2.7×10^{-8}	-7.57	[2]
59	0.415	1.139	1.0×10^{-7}	-7.00	[2]
59	0.415	1.318	0.92×10^{-6}	-6.04	[2]
62	0.435	0.848	3.2×10^{-7}	-6.50	[2]
64	0.435	1.019	1.3×10^{-7}	-6.89	[2]

Figure 7-2A and B. BETA-ZIRCONIUM
Experimental creep data at
60 microns grain size

Homologous Temperature T/T_M	Log σ MPa	$\dot{\varepsilon}(Sec^{-1})$	Log $\dot{\varepsilon}$	Reference
0.59	0.438	1.258×10^{-5}	-4.9	Author's Data Appendix I
0.59	0.838	2.138×10^{-4}	-3.67	Author's Data Appendix I
0.615	0.438	1.41×10^{-5}	-4.85	Author's Data Appendix I
0.615	0.838	3.311×10^{-4}	-3.48	Author's Data Appendix I

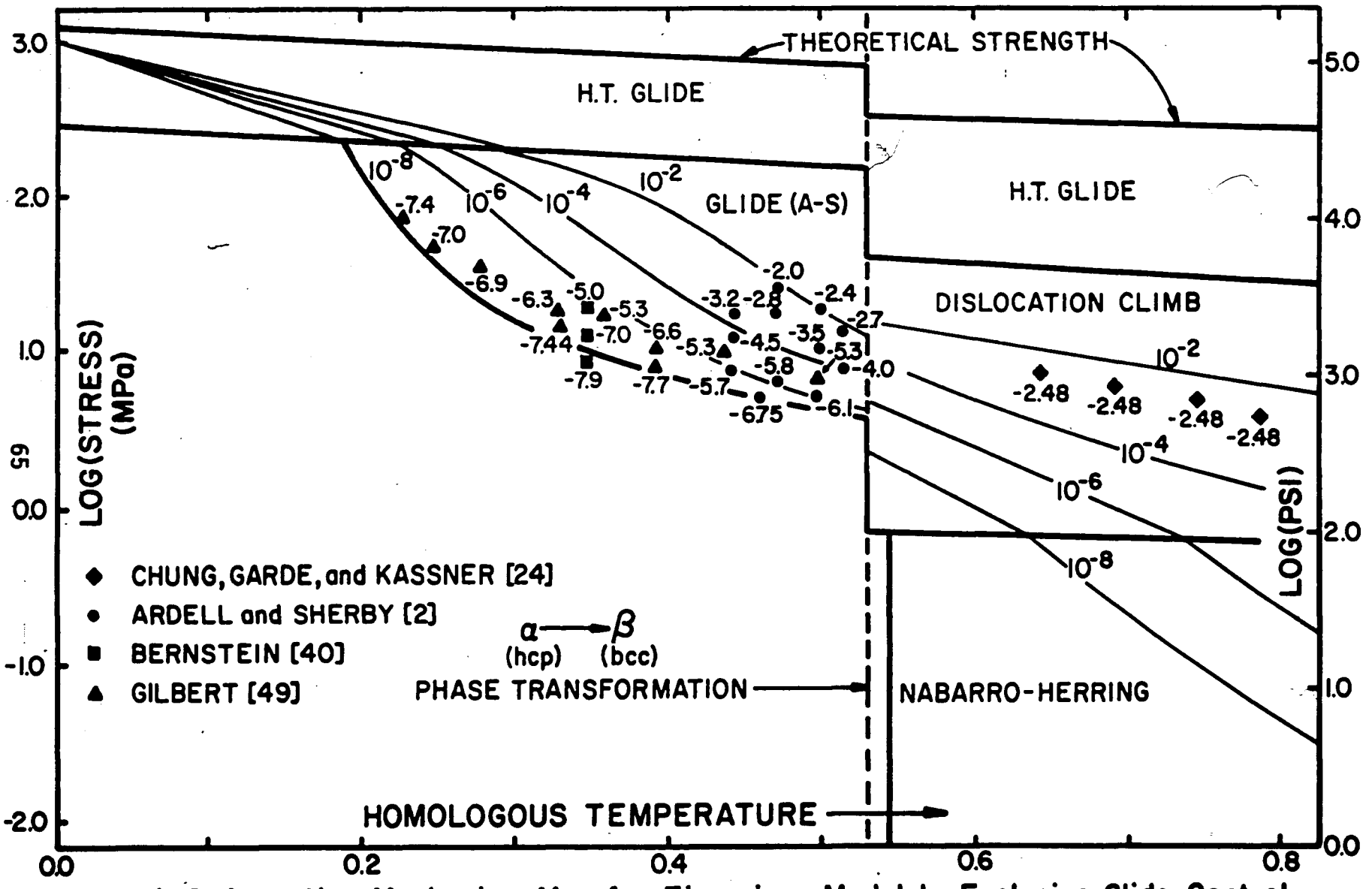

Fig.(7-3A)- Deformation Mechanism Map for Zirconium. Model I - Exclusive Glide Control. Grain Size = 300 microns

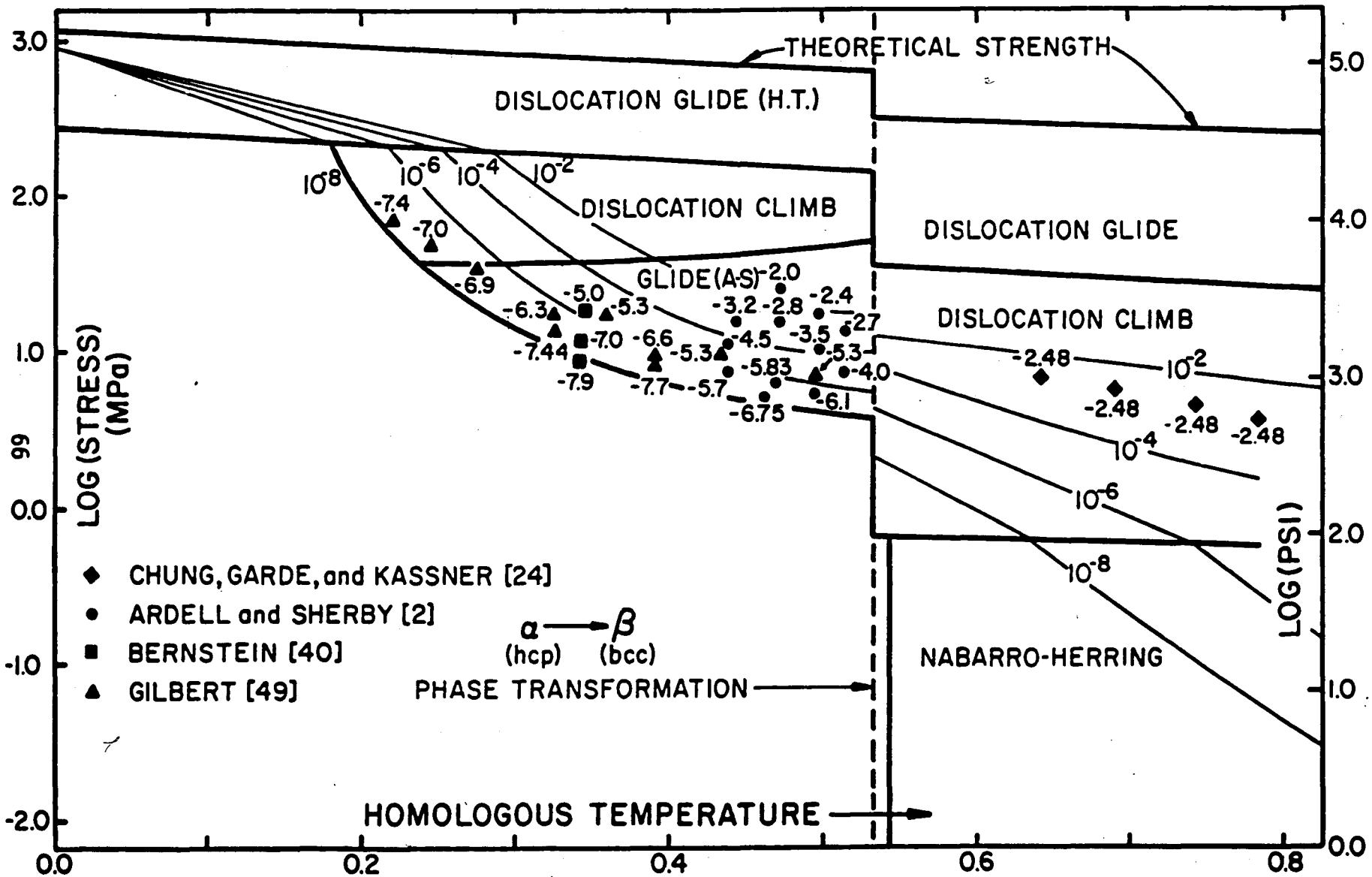

Fig.(7-3B)- Deformation Mechanism Map for Zirconium. Model II - Mixed Glide and Climb Control. Grain Size = 300 microns

Figures 7-3A and B. ALPHA-ZIRCONIUM
Experimental creep data at
300 microns grain size

Homologous Temperature	Log σ MPa	$\dot{\varepsilon}(Sec^{-1})$	Log $\dot{\varepsilon}$	Ref.
0.470	0.938	$1.5x10^{-6}$	-5.82	[52]
0.470	0.838	$1.8x10^{-7}$	-6.74	[52]
0.493	0.838	$8.3x10^{-7}$	-6.081	[52]
0.456	1.018	$2.0x10^{-6}$	-5.699	[52]
0.508	1.018	$1.0x10^{-4}$	-4.0	[52]
0.456	1.168	$3.0x10^{-5}$	-4.523	[52]
0.493	1.168	$3.0x10^{-4}$	-3.523	[52]
0.508	1.258	$2.0x10^{-3}$	-2.699	[52]
0.456	1.398	$6.0x10^{-4}$	-3.222	[52]
0.470	1.398	$1.5x10^{-3}$	-2.824	[52]
0.493	1.398	$4.0x10^{-3}$	-2.398	
0.470	1.578	$1.0x10^{-2}$	-2.0	[52]
0.385	0.988	$1.4x10^{-8}$	-7.85	[2]
0.385	1.138	$1.0x10^{-7}$	-7.00	[2]
0.385	1.418	$1.0x10^{-5}$	-5.00	[2]
0.399	1.348	$5.6x10^{-6}$	-5.252	[35]
0.315	1.698	$1.0x10^{-7}$	-7.00	[35]
0.372	1.198	$3.6x10^{-8}$	-7.444	[35]
0.372	1.348	$5.6x10^{-7}$	-6.252	[35]
0.292	1.828	$4.2x10^{-8}$	-7.377	[35]
0.412	0.978	$2.0x10^{-8}$	-7.699	[35]
0.412	1.108	$2.8x10^{-7}$	-6.552	[35]
0.490	0.978	$5.6x10^{-6}$	-5.252	[35]
0.455	1.108	$5.6x10^{-6}$	-5.252	[35]
0.341	1.538	$1.4x10^{-7}$	-6.854	[35]
0.315	1.828	$1.1x10^{-5}$	-4.959	[35]
0.250	1.928	$3.0x10^{-8}$	-7.523	[35]

In the case of maps for a grain size of 300 microns (Figures 7-3A and 7-3B), there is good agreement between experimental data and the computed maps. It is interesting to note that the constants for the dislocation creep equations are obtained from the data of Ardell and Sherby [2] at quite high temperatures, yet the data of Ardell as quoted in Bernstein [35] is in agreement with the deformation map at lower temperatures. This is true for both models, although a better fit is obtained in the case of "Mixed Glide and Climb" model.

The data points attributed to Gilbert et al. [52] are in excellent agreement except at very high stresses and/or low temperatures. Data below approximately 0.27 T_M do not agree well with map predictions; this may be attributable to the temperature effect on the diffusion coefficient which becomes small and thus causes the Ardell-Sherby model to break down.

In Figures (7-2A and 7B) experimental creep data for β-Zr that was generated in the laboratory at temperatures ranging from 975°C to 1040°C are included. The superimposed data yields a good approximation to the predictions of the maps.

Alloying elements are often added to zirconium in order to improve corrosion resistance. In theory, the deformation mechanisms of zirconium can be applied to zircaloy-2 (1.5 wt% Sn, 0.14% Fe, 0.10% Cr, 0.05% Ni, balance Zr). Therefore, if similar modelling is used, the same constitutive equations can be used by explicitly using new material constants that account for the alloy-

ing effects. The appropriate values are as listed in Table 5.2.

Maps of grain size 10 and 60 microns are shown in Figures 7-4 and 7-5. It can be seen that it has the same dominant mechanism regions and general shape as the map for zirconium. Experimental data points of Bernstein [35] and Duncombe and Busby [53] are plotted on the map for a grain size of 10 microns. The agreement with Bernstein's data for both models is excellent as expected; since several constants are derived from this data. The high stress steady-state data of Duncombe and Busby [53] falls in the correct region, but the strain rates change too fast for it to be a good fit. A plausible explanation is that there is a breakdown of the climb-controlled dislocation creep region as the high stress dislocation glide region is approached.

Data of Chung et al. [22] has been plotted on the maps for zircaloy-2 in the β-region. Although it falls in the correct region (diffusional creep) it does not conform to the predictions of the map. The strain-rates are off by over about two orders of magnitude, as can be seen in Figures 7-4A and B. It is surprising that the experimental data is considerably faster than that predicted.

The deformation maps at constant grain size for the two materials zirconium and zircaloy-2, show several similarities. One noticeable difference is in the Coble diffusional regime. Comparing the deformation maps at 10 microns grain size (Figures 7-1 and (7-4), equivalent creep rates for zircaloy-2 (Figure 7-4) appear to

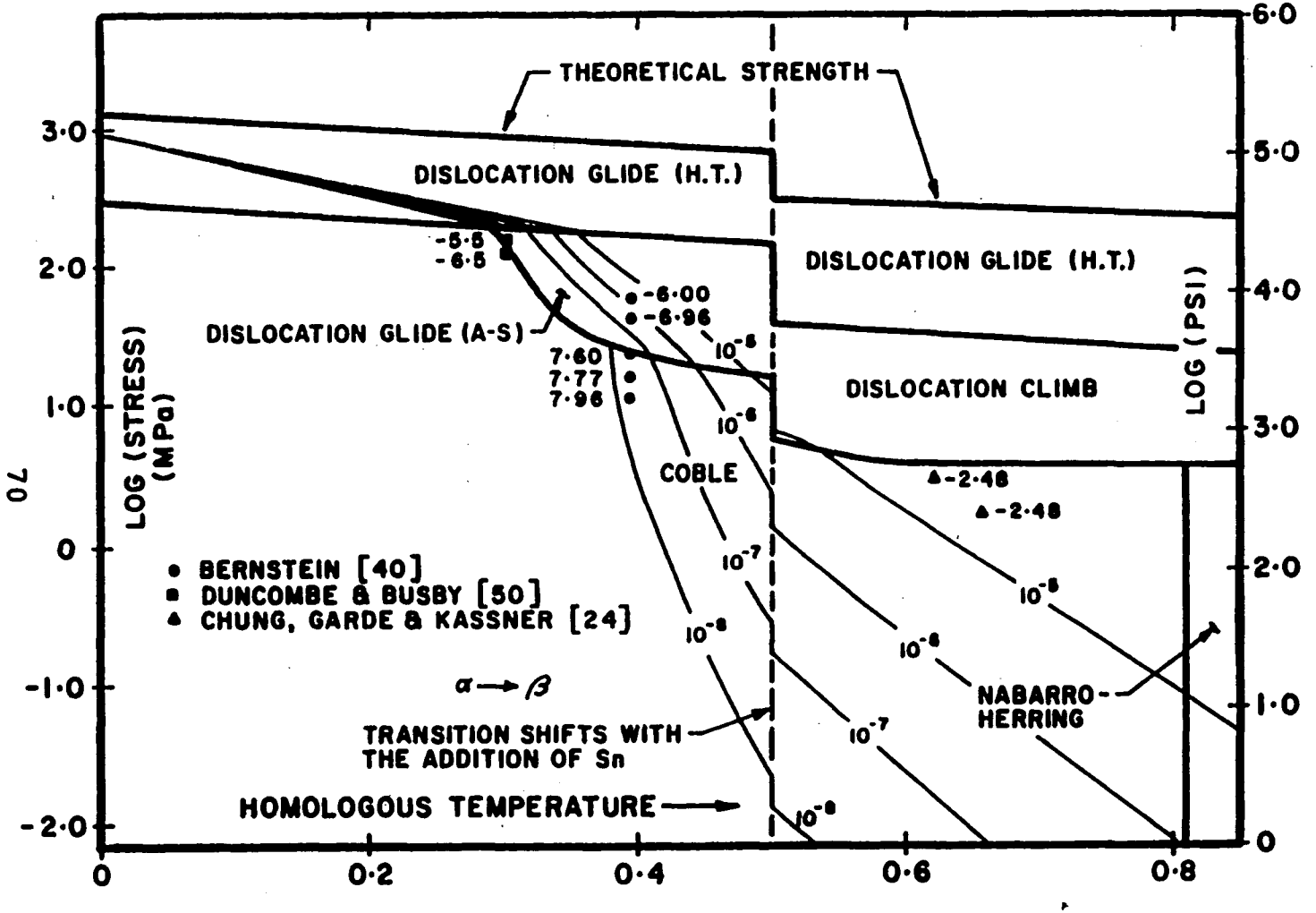

Fig. (7-4A) - Deformation Mechanism Map for Zircoloy-2.
Model I - Exclusive Glide Control. Grain Size = 10 microns.

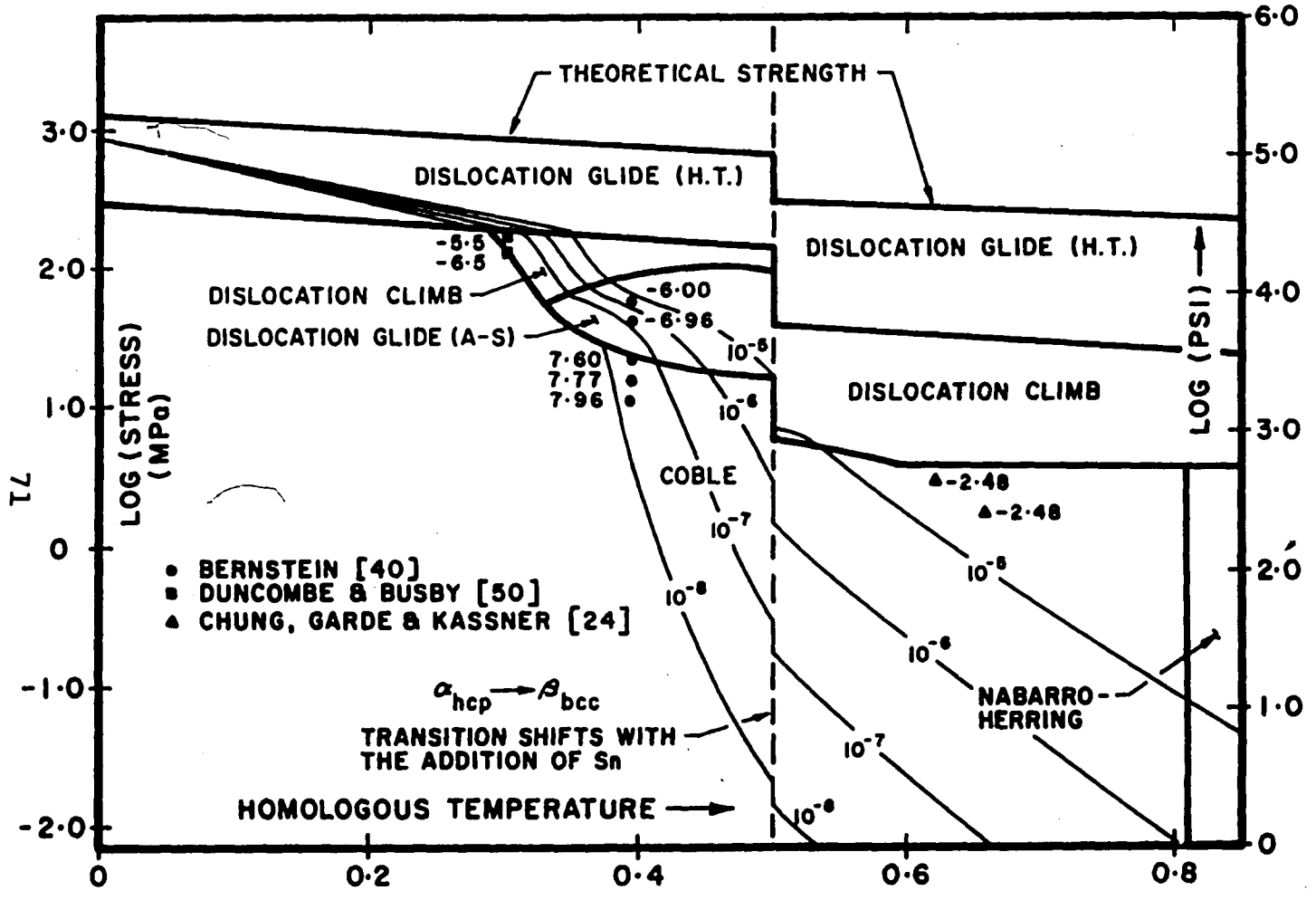

Fig. (7-4B) - Deformation Mechanism Map for Zircoloy-2.
Model II - Mixed Glide and Climb. Grain Size = 10 microns.

Figure 7-4A and B. BETA-REGION
Experimental creep data for
Zircaloy-2 of 10μ grain size

Homologous Temperature	Log σ MPa	$\dot{\epsilon}(Sec^{-1})$	Log $\dot{\epsilon}$	Reference
0.62	0.488	3.311×10^{-3}	-2.48	[22]
0.66	0.238	3.311×10^{-3}	-2.48	[22]

Figure 7-4A and B. ALPHA-REGION
Experimental creep data for
Zircaloy-2 for 10μ g.s.

Homologous Temperature	Log σ MPa	$\dot{\varepsilon}(Sec^{-1})$	Log $\dot{\varepsilon}$	Reference
0.385	1.03	$1.1x10^{-8}$	-7.959	[35]
0.385	1.158	$1.7x10^{-8}$	-7.770	[35]
0.385	1.318	$2.5x10^{-8}$	-7.602	[35]
0.385	1.558	$1.1x10^{-7}$	-6.959	[35]
0.385	1.788	$1.0x10^{-6}$	-6.000	[35]
0.303	2.238	$3.0x10^{-8}$	-7.523	[53]
0.303	2.298	$2.8x10^{-6}$	-5.553	[53]

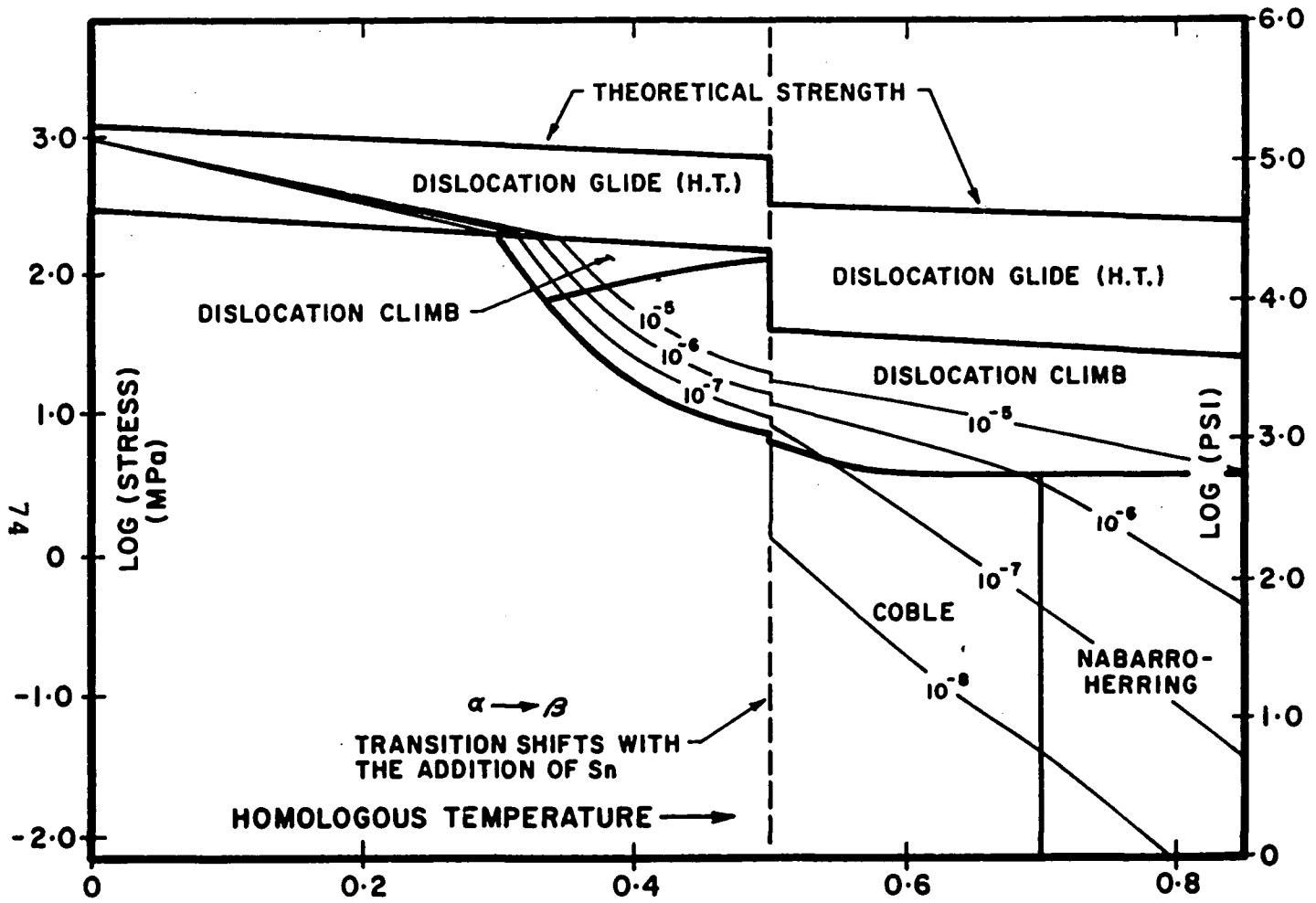

Fig. (7-5B)- Deformation Mechanism Map for Zircoloy - 2.
Model II - Mixed Glide and Climb. Grain Size = 60 microns.

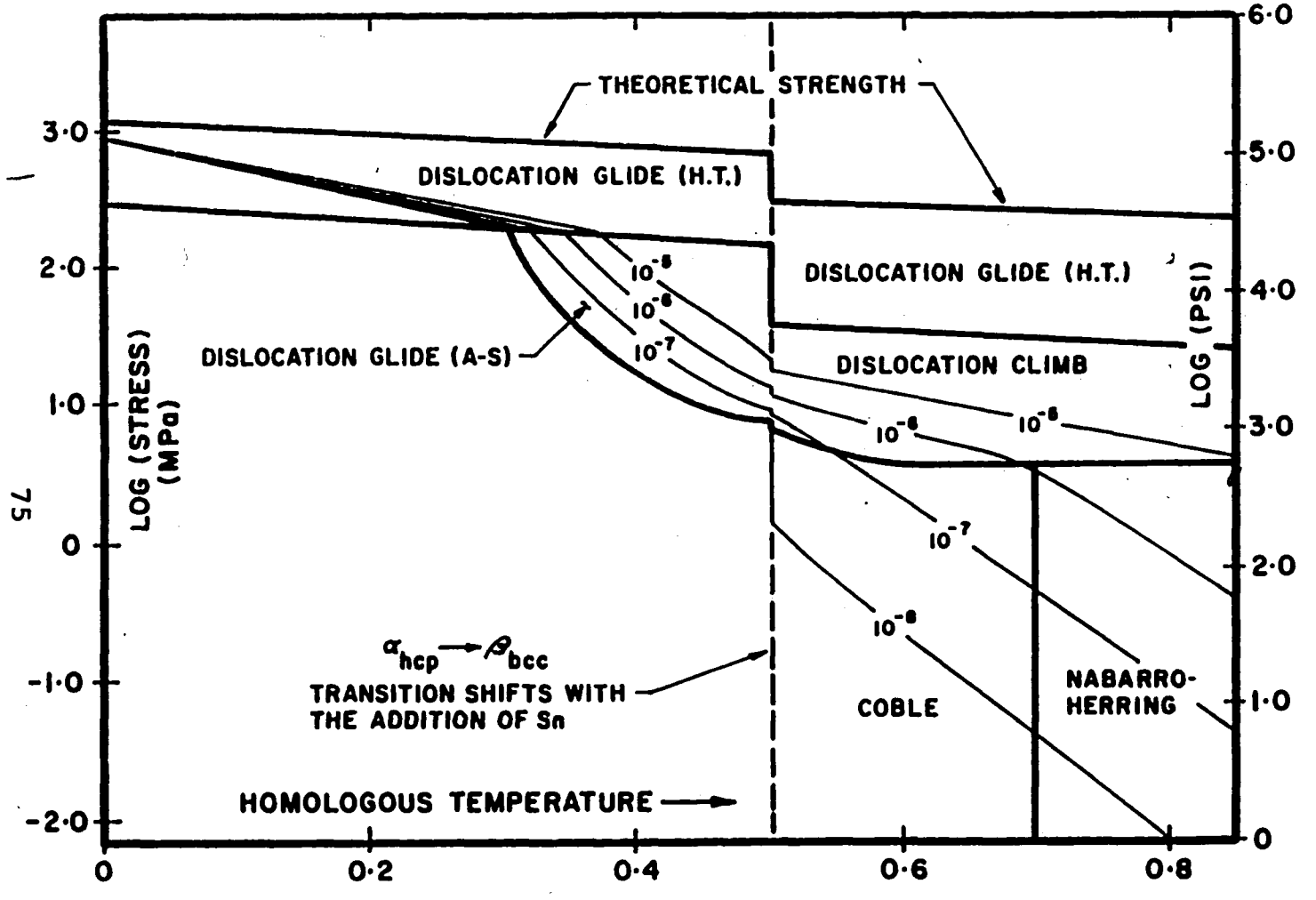

Fig. (7-5A)- Deformation Mechanism Map for Zircoloy-2.
Model I - Exclusive Glide Control. Grain Size = 60 microns.

be shifted to higher stresses or to higher temperatures within this regime, thus at a homologous temperature of 0.4 T_M, a creep rate of 10^{-7} sec^{-1} occurs at a stress level about two orders of magnitude higher in zircaloy-2 than in zirconium. A similar comparison may be noted at 60 microns (Figures 7-2 and 7-5). Another interesting difference lies in the position of the boundary between Coble and Nabarro-Herring creep regimes. The boundary shifts to the right for zircaloy-2 as compared to zirconium for grain sizes of 10, 60 microns. These effects are attributable to the difference in grain boundary diffusion coefficient since the grain boundary diffusion activation energy (Q_{gb}) is larger and the resulting diffusion coefficient is smaller in zircaloy-2 at a given temperature. The higher activation energy is due to the addition of tin in solid-solution, a result reported by Lyashenko et al. [47].

8. CONCLUSIONS

1. Deformation mechanism maps provide a good method for plotting creep behavior of a material over a wide range of stresses, temperatures and strain rates. This is because experimental data points can be plotted on the maps to test the validity of the models which are used. The maps provide a means for quantatively expressing the behavior of the material while at the same time increasing our physical understanding of the mechanisms involved.

Also, complex deformation behavior such as that demonstrated by dislocation glide (Peierls and Obstacle) can easily be incorporated into these deformation maps.

2. The models of Ardell and Sherby for dislocation creep (Mixed Glide and Climb, and Exclusive Glide) of alpha-zirconium yields a good approximation for creep behavior. The experimental data, however, of several investigators when superimposed on the computed maps fit the "Mixed Glide and Climb" better than the "Exclusive Glide" model. Two plausible explanations for it, may be considered:

a) If the temperature is greater than 0.5 T_M and the stress is high enough, the number of operative slip systems in the case of h.c.p. metals increases, so that glide becomes an easier process than climb.

b) When looking at the experimental results of Ardell and Sherby, one observes that the value of 'n' in the dislocation climb equation approaches 5.0 from 7.4 at high stress levels (see Figure 4-2) leading to lower climb rates. Thus, above a certain stress level glide controlled creep becomes faster than diffusion controlled creep and glide is no longer rate controlling, whereas at low stresses the reverse is true.

3. Phase transformations may be incorporated into the maps as demonstrated for the case of the $\alpha \rightarrow \beta$ transformation in zirconium.

4. For β-Zr, experimental data of Chung, Garde, and Kassner fits the predictions of the map within a reasonable degree of accuracy. Our own data when superimposed on the maps yields a good approximation to validate the predictions of the computed maps.

5. Comparison of the maps for zirconium and zircaloy-2 demonstrates that, especially in the Coble creep regime, at a given condition of stress and temperature, the creep resistance of zircaloy-2 is significantly better than zirconium.

6. A study of the intermediate temperature models of Heritier et al. [3] (athermal creep) and Miller and Sherby [4] (solute drag) shows that the models are as yet inadequate to be incorporated into the deformation mechanism maps. The athermal model is "patchy" due to a lack of sufficient data and the solute drag model, being simulated lacks identifiable physical constants.

9. SCOPE FOR FURTHER WORK

As mentioned earlier, an important mechanism which should be included in the deformation mechanism maps to complete the picture

of creep deformation of zirconium occurs at intermediate temperatures between 550-800°K. The research work being conducted to arrive at an applicable constitutive equation incorporating identifiable physical constants is at present rather involved and complex. The equation presented for "athermal" creep by Heritier et al. [3] is

$$\tau_a = \frac{\mu b}{fr} \tag{9.1}$$

where

μ = shear modulus

b = Burger's vector

f = a geometrical constant, which is related to the shape of the obstacle

r = dislocation segment length

τ_a = athermal stress

Both f and r have a range of values and depending on the values chosen, a band on the stress-temperature deformation map will be produced. However, the suitability of the equation and its effectiveness in predicting a deformation map compatible with experimental values, needs to be examined.

It has been known that texture does influence the creep rate of a material. The degree of texture induced by cold working zirconium is associated with the degree of alignation of the h.c.p. basal poles of zirconium crystals. The degree of alignation and

its influence on creep properties has been studied by a limited number of authors [54,55]. Kallstron et al. [57] have determined that the creep rate is lower in the transverse direction than in the longitudinal direction. Also, more radial basal poles give lower creep strength than transverse basal pole alignation. They have also attempted to develop an equation that will quantitatively measure the effects of texture. However, how this equation can be included in normal creep equations deserves a closer examination. It may be argued that the texture effect is small in comparison to the effects of cold working and annealing. However small the effects may be, they are measurable and certain crucial parts of a reactor definitely do need extremely accurate designing criteria.

Finally, irradiation creep is probably the most important mechanical property that deserves attention. If one can model the deformation due to irradiation alone it would be of immense value. Nichols has attempted to characterize irradiation affects in the temperature and stress range of importance to a nuclear reactor.

The effect of neutron irradiation at temperatures less than 300°C on the mechanical properties of zirconium and its alloys is largely dependent on the specific conditions of the experiments. For example, some experimental tests have shown a decrease in creep rate, while others have indicated an increase in creep rate. Theoretically, it would seem that neutron irradiation will enhance creep rates, simply because of the fact that vacancies and inter-

stitials are produced during irradiation. However, diffusion is not the dominant mode of deformation at low temperatures, which means an alternative mechanism may have a greater influence on the creep rate. This introduces the question of increasing the diffusion rate by some means (by irradiation in this case) such that it is equal to or greater than the value normally obtained at $T > 0.5\ T_M$, so that diffusion controlled creep may be dominant.

The flux level required to yield enhanced diffusion rates can be roughly estimated to be ~10^{14} nv (>1 MeV) (Schock, et al. [37]). This value is important because it is at this level that neutron irradiation first begins to have an effect on the diffusion rate. For example, Holmes et al. [38] have conducted tests on cold-worked zircaloy to estimate differences in in-pile and out-of-pile creep rates. The tests were conducted at relatively high temperatures and stresses, but low neutron flux levels. Consequently, the thermal creep rates were high and the effects of radiation enhanced creep were low. The results proved to be inconclusive as the investigators [38] could notice no significant difference.

In addition to the question of what effect irradiation will have on normal (or thermal) creep mechanisms, the possibility exists of radiation creep mechanisms completely unrelated to thermal creep and operating quite independently. One such model has been proposed by Roberts and Cottrell [39] to account for radiation creep of alpha-uranium over the regime where radiation growth (i.e. dimen-

sional change without an applied stress) is observed to occur. Zircaloy also shows radiation growth (Nichols [40] et al.) so that the Roberts-Cottrell [38] mechanism may apply for it.

A reasonably accurate model for this phenomena has been proposed by Nichols [41]. The approach is semi-empirical and satisfies observed experimental data within a comfortable margin.

At low stress levels, in-pile creep at reactor temperatures appears to coincide approximately with out-of-pile creep tests at the same temperature and stress. Therefore, the author [41] assumed that during irradiation the total observed creep rate at low stresses is the summation of that which would occur out-of-pile (thermal), plus an irradiation growth term, plus an independent radiation creep rate. In both the low-stress and high-stress regimes, the strain rate can be expressed as:

$$\dot{\varepsilon}_T = \dot{\varepsilon}_{th} + \dot{\varepsilon}_{IRRAD}$$

where

$\dot{\varepsilon}_T$ = total in-pile creep rate

$\dot{\varepsilon}_{th}$ = thermal creep rate

$\dot{\varepsilon}_{IRRAD} = (A + B\sigma)\phi$

A, B = constants = f(T,ε, structure, texture)

σ = applied stress

ϕ = fast neutron flux (>1MeV)

At low stresses the first term ($\dot{\varepsilon}_{th}$) is small and the second term dominates; at high stresses, $\dot{\varepsilon}_{th}$ dominates.

In the intermediate stress region, the irradiation contribution to the total strain rate includes a third term and is given by:

$$\dot{\varepsilon}_{IRRAD} = (A + B\sigma)\phi + \frac{C\pi\sigma^4\lambda^2 D^*(\phi)}{(8\sqrt{2})h\mu^3 KT}$$

where

C = constant

λ = average spacing between barriers

D^* = in-pile diffusion coefficient

$= D_{th} + \dot{N}\overline{X^2}$

D_{th} = thermal diffusion coefficient

$\dot{N}$ = rate of vacancy production due to flux

$\overline{X^2}$ = root mean square distance between sinks

h = the height of barrier to dislocation motion

μ = shear modulus

In this intermediate stress range Nichols includes both the thermal and irradiation components in a complex series-parallel combination form. For the purpose of the present maps we have ignored this more complex approach.

More work in this direction will be of definite usefulness to nuclear and design engineers.

REFERENCES

1. Knorr, D and Notis, M. R., "Deformation Mechanism Mapping of α-Zirconium and Zircaloy-2," Journal of Nuclear Materials, 56 (1) (1975), p. 18.

2. Ardell, A. J. and Sherby, O. D., "The Steady State Creep of Polycrystalline Alpha Zirconium at Elevated Temperature," Trans. ASME, 239 (1967), pp. 1547-1556.

3. Heritier, B., Luton, M. J., and Jonas, J. J., "The Transition Between Thermally Activated and Athermal Flow in Polycrystalline Alpha-Zirconium," Metal Science, 8 (1976), pp. 41-48.

4. Miller, A. K. and Sherby, O. D., "Development of the Materials Code, MATMOD," First Quarterly Progress Report, EPRI Sponsored, Stanford University, California, May 1 - July 31 (1975).

5. Frost, H. J. and Ashby, M. F., "A Second Report on Deformation Mechanism Maps," Harvard University, Cambridge, Massachusetts, August 1973.

6. Nabarro, F. R. N., "Conference on Strength of Solids," University of Bristol (1947), pp. 75-90.

7. Coble, R. L., "A Model for Boundary Diffusion Controlled Creep in Polycrystalline Materials," Journal of Applied Physics, 34 (1963), p. 1679.

8. Ashby, M. F., "Boundary Defects, and Atomistic Aspects of Boundary Sliding and Diffusional Creep," Surface Science, 31 (1972), pp. 498-542.

9. Ashby, M. F. and Verrall, R. A., "Diffusion Accommodated Flow and Superplasticity," Acta Metallurgica, 21 (1973), p. 149.

10. Mukherjee, A. K., Bird, J. E. and Dorn, J. E., "Creep of Metals at High Temperature," American Society of Metals, Transactions Quarterly, 62 (1969), pp. 155-179.

11. Stocker, R. L. and Ashby, M. F., "On the Empirical Constants in the Dorn Equation," Scripta Metallurgica, 7 (1973), pp. 115-120.

12. Weertman, J., "An Empirical Relation Defining the Stress Dependence of Minimum Creep Rate in Metals," Transactions AIME, 227 (1963), p. 1474.

13. Nabarro, F. R. N., "Steady-State Diffusional Creep," Phil. Mag., 8 (1967), p. 231.

14. Kidson, G. V., "Mechanism of Diffusion in Beta-Zirconium, Beta-Titanium and Gamma-Uranium," Diffusion in b.c.c. Metals, ASM, Metals Park, Ohio (1965).

15. Guyot, P. and Dorn, J. E., "Critical Review of Pieriel's Mechanism," Canadian Journal of Physics, 45 (1967), p. 983.

16. Kocks, U. F., Argon, A. S. and Ashby, M. F., "Thermodynamics and Kinetics of Slip," Progress in Materials Science, 19 (1974), pp. 1-281.

17. Evans, A. G. and Rawlings, R. D., "Thermally Activated Deformation of Crystalline Materials," Physics Status Solidi, 34 (1969), p. 9.

18. Klahn, D., Mukherjee, A. K. and Dorn, J. E., "Strain Rate Effects," Second International Conference on the Strength of Metals and Alloys, ASM, Asilomar, California, 3 (1970), p. 951.

19. Miller, A. K. and Sherby, O. D., "Development of the Materials Code, MATMOD," Third Quarterly Progress Report, EPRI Sponsored, Stanford University, Stanford, California, Nov. 1 - Jan. 31, (1975).

20. Mackenzie, J. K., "On the Deformation of b.c.c. Metals," Proceedings of the 41st Conference of the American Institute of Mining, Metallurgical and Petroleum Engineers, New York, vol. 41 (1958), pp. 211-217.

21. Surek, T., Kuon, L. G., Luton, M. J. and Jones, J. J., "John E. Dorn Memorial Symposium on Rate Process in Plastic Deformation," October 16, 1972, Cleveland, Ohio.

22. Chung, H. M., Garde, A. M. and Kassner, T. F., "Mechanical Properties of Zircaloy Containing Oxygen," Light Water Reactor Safety Research Program: Quarterly Progress Report, April - June 1975, Argonne National Laboratory, Argonne, Illinois.

23. Discussions with Dr. M. F. Ashby, November 1975, Lehigh University, Bethlehem, Pa.

24. Shaw, B., "Twinning and Low Temperature Mechanical Properties of Polycrystalline Niobium and Molybdenum," Trans. AIME, 13 (3), (1967), p. 294.

25. Garde, A. M., Aigeltinger, E., Woodruff, B. N., and Reed-Hill, R. E., "Concerning the Strength of Dynamic Strain Aging in Zirconium," Metallurgical Transaction Part A, 6A (1975), p. 1183.

26. Barrett, C. R. and Sherby, O. D., "Effect of Grain Size and Annealing Treatment on Steady State Creep of Copper," Trans. AIME, 239 (1967), p. 170.

27. Dorn, J. E., "Strain-Rate Measurements at High Temperatures," in Creep Fracture of Metals at High Temperatures, HMSO, London (1956), p. 89.

28. Weertman, J., "Steady State Creep Through Dislocation Climb," Journal of Applied Physics, 28 (1957), p. 362.

29. Barrett, C. R. and Nix, W. D., "A Model for Steady-State Creep Based on Motion of Screw Dislocations," Acta Metallurgica, 13 (1965), p. 1247.

30. Burke, P. M. and Sherby, O. D., "Mechanical Behavior of Crystalline Solids at Elevated Temperatures," Progress in Materials Science, 13 (1968), p. 325.

31. Garofalo, F., "An Empirical Relation Defining the Stress Dependence of Minimum Creep Rate in Metals," Trans. AIME, 227 (1963), p. 351.

32. Gilman, W., "Dislocation Mobility in Crystals," Journal of Applied Physics, 36 (1965), p. 3195.

33. Soo, P. and Higgins, G. T., "Deformation of Zirconium-Oxygen Single Crystals," Acta Metallurgica, 16 (1968), p. 177.

34. Sashtry, D. H., Prasad, Y. V. R. K. and Vasu, K. I., "Evaluation of Rate-Controlling Obstacles for Low Temperature Deformation of Zirconium," Journal of Material Science, 6 (1971) p. 332.

35. Bernstein, I. M., "Diffusional Creep in Zirconium and Certain Zirconium Alloys," Trans. AIME, 239 (1967), p. 1518.

36. Cotrell, A. H., "Interactions of Dislocations and Solute Atoms," in Relation of Properties to Microstructures, ASM (1953), pp. 131-162.

37. Schoeck, G., "Influence of Irradiation on Creep," Journal of Applied Physics, 29 (1958), p. 112.

38. Holmes, J. J., Williams, J. A., Nyman, D. H. and Tobin, J. C., "Flow and Fracture of Metals and Alloys in Nuclear Environments," ASTM, Special Technical Publication 380, Philadelphia, Pa. (1965), p. 385.

39. Roberts, A. C. and Cotrell, A. H., "Creep of Alpha Uranium During Irradiation with Neutrons," Philosophical Magazine, Ser. 8, vol. 1 (1956), p. 711.

40. Nichols, F. A., Kearns, J. J. and McCawley, J. E., "Effect of Alpha-Beta Phase Constitution on Superplasticity and Strength of Zircaloy-4," Journal of Nuclear Materials, 61 (2), (1976), pp. 169-184.

41. Nichols, F. A., "Theory of the Creep of Zircaloy During Neutron Irradiation," Journal of Nuclear Materials, 30 (1969), pp. 249-270.

42. Smoak, R. and Notis, M. R., "Deformation Behavior of MGAL 204 During Pressure Sintering," American Ceramic Society Bulletin, 53 (4), (1974), p. 319.

43. Mohamed, F. A. and Langdon, T. G., "Deformation Mechanism Maps Based on Grain Size," Metallurgical Transactions, 5 (11), (1974), pp. 2339-2345.

44. Notis, M. R., "Deformation Mechanism Maps - A Review with Applications," Department of Metallurgy and Materials Science, Lehigh University, Bethlehem, Pa. (1974).

45. Metals Handbook, ASM, vol. 8 (1973), p. 336.

46. Bocek, M., "Superplasticity in Zircaloy-2," Journal of Nuclear Materials, 62 (1976), p. 26.

47. Lyashenko, V. S., Bykov, V. N. and Pavlinov, L. V., "A Study of Self-Diffusion in Zirconium and its Alloys with Tin," Physics of Metals and Metallography, (USSR, English Translation by Coleman), 8 (1959), pp. 40-46.

48. Koster, V. W., "Die Temperaturabhangigkeit des Elastizitatsmoduls Reiner Metalle," Zeitschrift fur Metall Kunde, 39 (1948), p. 1.

49. Reactor Handbook, 2nd Edition, Interscience, New York, Vol. 1 - Materials (1960), pp. 708-738.

50. Krishamachari, V., "Creep Recovery of Rutile Under Reduced Stress," Doctoral Thesis, Iowa State University, Ames, Iowa, 1971.

51. Hilliard, J. E., "Comment on Cahn's Diffusion Equation," Scripta Metallurgica, 6 (1972), p. 909.

52. Gilbert, E. R., Duran. S. A. and Bennet, A. L., "Creep of Zirconium from 50°C to 850°C," Application Related Phenomena for Zirconium and its Alloys, ASTM STP 458 (1969), pp. 210-225.

53. Duncombe, E. and Busby, C. C., "FLIC and CYGRO Parameters for Out-of-Pile, Unirradiated, Annealed Zircaloy," WAPD-FD(R)-73, March (1973).

54. Tyson, W. R., "Strengthening of h.c.p. Zr, Ti, and Hf by Interstitial Solutes - A Review," Canadian Met. Quart., 6 (1968), p. 301.

55. Mills, D. and Craig, G. B., "Plastic Deformation of Zirconium-Oxygen Alloy Single Crystals in Range 77°K to 950°K," Transaction Met. Soc. AIME, 242 (1968), p. 1881.

56. Fisher, E. S. and Dever, D., "The Single Crystal Elastic Moduli of Beta-Titanium and Titanium-Chromium Alloys," The Science Technology and Application of Titanium, Oxford and New York: Pergamon Press (1970).

57. Kallstrom, K., Anderson, T. and Hofrenstam, A., "Creep Strength of Zr Tubing at 400°C as Dependent on Metallurgical Structure and Texture," Zirconium in Nuclear Applications, ASM (1974).

APPENDIX I

Tabulation of Experimental Creep Data for β-Zirconium

Table A.1

ZR#1	Conditions (†)
	Test temperature = 1000°C = 0.596 T_M
	Annealing temperature = 1050°C
	Time at annealing temperature = 20 mins.
	Temperature fluctuation = ±1°C
	Stabilizing time at test temp = 2½ hours
	Initial grain size = 58 microns
	Final grain size = 60 microns

† All the data presented here is in the F.P.S. system. This has been done in order to avoid a loss of accuracy in converting to the S.I. units. However the output is dimensionless and hence there is no effect on the data presented in the Deformation Mechanism Maps.

ZR#1

Time Minutes	$\Delta\ell$ Elongation (inches)	ε Strain	$\dot{\varepsilon}$/sec. Strain Rate	L_o (inches)	A_o (square in.)	σ Stress (psi)	Remarks
0	0.000001			0.199	0.0099	300	Average strain rate for last 4 readings
5	0.00004	2.01×10^{-4}				400	
10	0.00005	2.51×10^{-4}	1.67×10^{-7}			400	
15	0.00071	3.57×10^{-3}	1.11×10^{-5}			400	$\dot{\varepsilon}$/sec = 1.3375×10^{-5}
20	0.00145	7.31×10^{-3}	1.257×10^{-5}			400	$\log(\dot{\varepsilon}) = -4.873$
25	0.00229	11.52×10^{-3}	1.403×10^{-5}			400	$\log(\sigma) = 2.60$
30	0.00321	16.26×10^{-3}	1.58×10^{-5}			400	
0				0.10581	0.0100	1000	Average strain rate for 5 readings
5	0.00136	6.97×10^{-3}					
10	0.01622	8.65×10^{-2}	2.65×10^{-4}				
15	0.02822	1.56×10^{-1}	2.32×10^{-4}				$\dot{\varepsilon}$/sec = 2.14×10^{-4}
20	0.038224	2.17×10^{-1}	2.03×10^{-4}				$\log(\dot{\varepsilon}) = -3.67$
25	0.04772	2.79×10^{-1}	2.07×10^{-4}				$\log(\sigma) = 3.00$
30	0.05474	3.28×10^{-1}	1.63×10^{-4}				

Table A.2

ZR#2	Conditions (†)
	Test temperature = 1040°C = 0.615 T_M
	Annealing temperature = 1100°C
	Time at annealing temperature = 20 mins.
	Stabilizing time at test temp = 50 mins.
	Temperature fluctuation = $\pm$1°C
	Initial grain size = 58 microns
	Final grain size = 65 microns

†All the data presented here is in the F.P.S. system. This has been done in order to avoid a loss of accuracy in converting to the S.I. units. However the output is dimensionless and hence there is no effect on the data presented in the Deformation Mechanism Maps.

ZR#2

Time Minutes	$\Delta\ell$ Elongation (inches)	ε Strain	$\dot{\varepsilon}$/sec. Strain Rate	L_o (inches)	A_o (square in.)	σ Stress (psi)	Remarks
0	0.0013	6.5×10^{-3}		0.200	0.0097	400	Average strain rate for 5 readings
5	0.0025	12.51×10^{-3}	2.02×10^{-5}			400	
10	0.0035	17.67×10^{-3}	1.70×10^{-5}			400	
15	0.00432	21.83×10^{-3}	1.39×10^{-5}			400	$\dot{\varepsilon}$/sec = 1.41×10^{-5}
20	0.00495	25.06×10^{-3}	1.08×10^{-5}			400	$\log(\dot{\varepsilon}) = -4.99$
25	0.00565	28.66×10^{-3}	1.20×10^{-5}			400	$\log(\sigma) = 2.60$
30	0.00628	31.90×10^{-3}	1.08×10^{-5}			400	
0	0.0015	7.72×10^{-3}		0.1951	0.0099	1000	Average strain rate for 5 readings
5	0.01754	94.20×10^{-3}	2.88×10^{-4}			1000	
10	0.03477	196.0×10^{-3}	3.39×10^{-4}			1000	
15	0.05229	312.0×10^{-3}	3.86×10^{-4}			1000	$\dot{\varepsilon}$/sec = 3.311×10^{-4}
20	0.06952	407.0×10^{-3}	3.17×10^{-4}			1000	$\log(\dot{\varepsilon}) = -3.48$
25	0.07733	504.8×10^{-3}	3.26×10^{-4}			1000	$\log(\sigma) = 3.0$

Table A.3

ZR#3	Conditions (†)
	Test temperature = 1030°C
	Annealing temperature = 1070°C
	Time at annealing temperature = 20 mins.
	Temperature fluctuation = ±1°C
	Stabilizing time at test temp = 30 mins.
	Initial grain size = 58 microns
	Final grain size = 76 microns

†All the data presented here is in the F.P.S. system. This has been done in order to avoid a loss of accuracy in converting to the S.I. units. However the output is dimensionless and hence there is no effect on the data presented in the Deformation Mechanism Maps.

ZR#3

Time Minutes	$\Delta\ell$ Elongation (inches)	ε Strain	$\dot{\varepsilon}$/sec. Strain Rate	L_o (inches)	A_o (square in.)	σ Stress (psi)	Remarks
0	0.00015	0.75×10^{-3}		.1998	.00967	1000	
5	0.00024	1.20×10^{-3}					Average strain rate
10	0.00034	1.70×10^{-3}					
15							
20	0.00036	1.8×10^{-3}					$\dot{\varepsilon}$/sec = 6.7×10^{-7}
							log(1000) = 3.0
0	0.0004	2.0×10^{-3}		.19959		2000	
5	0.00062	3.1×10^{-3}	3.67×10^{-6}				Average strain rate
10	0.0078	3.9×10^{-3}	2.67×10^{-6}				
15	0.00083	4.2×10^{-3}	1.0×10^{-6}				$\dot{\varepsilon}$/sec = 1.75×10^{-6}
20	0.00093	4.7×10^{-3}	1.66×10^{-6}				log(2000) = 3.3
0	0.0007	3.5×10^{-3}		.1991		2500	
5	0.00825	4.3×10^{-3}	2.66×10^{-6}				Average strain rate
10	0.00097	4.9×10^{-3}	2.0×10^{-6}				
15	0.00104	5.2×10^{-3}	1.0×10^{-6}				$\dot{\varepsilon}$/sec = 1.9×10^{-6}
20	0.00119	6.0×10^{-3}	2.67×10^{-6}				log(2500) = 3.398
0	0.0007	3.5×10^{-3}		.19861		3000	
5	0.00087	4.4×10^{-3}	3.7×10^{-6}				Average strain rate
10	0.0010	5.1×10^{-3}	2.3×10^{-6}				
15	0.00105	5.3×10^{-3}	67.0×10^{-6}				$\dot{\varepsilon}$/sec = 1.3×10^{-6}
20	0.00110	5.6×10^{-3}	1.0×10^{-6}				log(3000) = 3.477

ZR#3 (Continued)

Time Minutes	$\Delta\ell$ Elongation (inches)	ε Strain	$\dot{\varepsilon}$/sec. Strain Rate	L_o (inches)	A_o (square in.)	σ Stress (psf)	Remarks
0	0.000875	$.0044 \times 10^{-3}$		.19821		3500	Average strain rate
5	0.00108	$.0055 \times 10^{-3}$	3.7×10^{-6}				$\dot{\varepsilon}$/sec = 1.9×10^{-6}
10	0.00124	$.0063 \times 10^{-3}$	2.7×10^{-6}				log(3500) = 3.544
15	0.00134	$.0068 \times 10^{-3}$	1.7×10^{-6}				
20	0.00142	$.0072 \times 10^{-3}$	1.4×10^{-6}				
0	0.00092	4.7×10^{-3}		.197665		4000	Average strain rate
5	0.00114	5.8×10^{-3}	3.7×10^{-6}				$\dot{\varepsilon}$/sec = 1.8×10^{-6}
10	0.00129	6.5×10^{-3}	2.4×10^{-6}				log(4000) = 3.602
15	0.00139	7.1×10^{-3}	2.0×10^{-6}				
20	0.00145	7.4×10^{-3}	1.0×10^{-6}				
0	0.0013	6.6×10^{-3}		.197135		4500	Average strain rate
5	0.00145	7.4×10^{-3}	2.7×10^{-6}				$\dot{\varepsilon}$/sec = 2.4×10^{-6}
10	0.00161	8.2×10^{-3}	2.7×10^{-6}				log(4500) = 3.653
15	0.00175	8.9×10^{-3}	2.3×10^{-6}				
20	0.00187	9.5×10^{-3}	2.0×10^{-6}				

Table A.4

ZR#4	Conditions (†)
	Test temperature = 985°C
	Annealing temperature = 1050°C
	Time at annealing temperature = 20 mins.
	Temperature fluctuation = ±1°C
	Stabilizing time at test temp = 30 mins.
	Initial grain size = 58 microns
	Final grain size = 61 microns

†All the data presented here is in the F.P.S. system. This has been done in order to avoid a loss of accuracy in converting to the S.I. units. However the output is dimensionless and hence there is no effect on the data presented in the Deformation Mechanism Maps.

ZR#4

Time Minutes	$\Delta\ell$ Elongation (inches)	ε Strain	$\dot{\varepsilon}$/sec. Strain Rate	L_o (inches)	A_o (square in.)	σ Stress (psi)	Remarks
0	.0002	1.0×10^{-3}		.1995	.010	1000	Average strain rate
5	.00029	1.45×10^{-3}	1.5×10^{-6}				
10	.00037	1.86×10^{-3}	1.37×10^{-6}				$\dot{\varepsilon}$/sec = 1.34×10^{-6}
15	.00044						log(1000) = 3.0
20	.00053	2.66×10^{-3}	2.2×10^{-6}				
0	.00054	2.7×10^{-3}		.19917		2000	Average strain rate
5	.00069	3.5×10^{-3}	2.7×10^{-6}				
10	.00075	3.77×10^{-3}					$\dot{\varepsilon}$/sec = 1.14×10^{-6}
15	.00082	4.13×10^{-3}	1.2×10^{-6}				log(2000) = 3.3
20	.0009	4.53×10^{-3}	1.3×10^{-6}				
0	.0006	3.0×10^{-3}		.19881		2500	Average strain rate
5	.00074	3.73×10^{-3}	2.4×10^{-6}				
10	.00082	4.13×10^{-3}	1.3×10^{-6}				$\dot{\varepsilon}$/sec = 1.17×10^{-6}
15	.00089	4.49×10^{-3}	1.2×10^{-6}				log(2500) = 3.398
20	.00095	4.79×10^{-3}	1.0×10^{-6}				
0	.00061	3.08×10^{-3}		.19846		3000	Average strain rate
5	.00082	4.14×10^{-3}	3.53×10^{-6}				
10	.00083	4.19×10^{-3}	16.67×10^{-6}				$\dot{\varepsilon}$/sec = 3.9×10^{-7}
15	.00086	4.34×10^{-3}	50.0×10^{-6}				log(3000) = 3.477
20	.00089	4.49×10^{-3}	50.0×10^{-6}				

ZR#4(continued)

Time Minutes	$\Delta\ell$ Elongation (inches)	ε Strain	$\dot{\varepsilon}$/sec Strain Rate	L_o (inches)	A_o (square in.)	σ Stress (psi)	Remarks
0	.00088	4.45×10^{-3}		.19818		3500	Average strain rate
5	.00102	5.16×10^{-3}	2.37×10^{-6}				
10	.0011	5.57×10^{-3}	1.37×10^{-6}				$\dot{\varepsilon}$/sec = 1.46×10^{-6}
15	.00118	5.97×10^{-3}	1.33×10^{-6}				log(3500) = 3.544
20	.0012	6.47×10^{-3}	1.07×10^{-6}				
0	.00105	5.32×10^{-3}		.19786		4000	Average strain rate
5	.00133	6.74×10^{-3}	4.73×10^{-6}				
10	.00142	7.20×10^{-3}	1.53×10^{-6}				$\dot{\varepsilon}$/sec = 1.31×10^{-6}
15	.0015	7.61×10^{-3}	1.37×10^{-6}				log(4000) = 3.602
20	.00156	7.92×10^{-3}	1.03×10^{-6}				
0	.0013	6.6×10^{-3}		.19735		4500	Average strain rate
5	.00141	7.17×10^{-3}	1.9×10^{-6}				
10	.0015	7.63×10^{-3}	1.53×10^{-6}				$\dot{\varepsilon}$/sec = 1.24×10^{-6}
15	.00156	7.94×10^{-3}	1.03×10^{-6}				log(4500) = 3.653
20	.00.63	8.29×10^{-3}	1.167×10^{-6}				
0	.0015	7.64×10^{-3}		.19702		5000	Average strain rate
5	.00162	8.26×10^{-3}	2.07×10^{-6}				
10	.00169	8.62×10^{-3}	1.20×10^{-6}				$\dot{\varepsilon}$/sec = 1.24×10^{-6}
15	.00179	9.13×10^{-3}	1.70×10^{-6}				log(5000) = 3.7
20	.00184	9.38×10^{-3}	8.30×10^{-6}				

Table A.5

ZR#5	Conditions (†)
	Test temperature = 975°C
	Annealing temperature = 1055°C
	Time at annealing temperature = 20 mins
	Temperature fluctuation = ±1°C
	Stabilizing time at test temp = 30 mins
	Initial grain size = 58 microns
	Final grain size = 65 microns

†All the data presented here is in the F.P.S. system. This has been done in order to avoid a loss of accuracy in converting to the S.I. units. However the output is dimensionless and hence there is no effect on the data presented in the Deformation Mechanism Maps.

ZR#5

Time Minutes	$\Delta\ell$ Elongation (inches)	ε Strain	$\dot{\varepsilon}$/sec. Strain Rate	L_o (inches)	A_o (square in.)	σ Stress (psi)	Remarks
0	.0012	6.0×10^{-3}		.2004	.01008	2000	Average strain rate
1	.0016	8.0×10^{-3}	33.6×10^{-6}				
6	.00256	12.9×10^{-3}	16.3×10^{-6}				$\dot{\varepsilon}$/sec = 7.0×10^{-6}
11	.00332	10.7×10^{-3}	12.6×10^{-6}				
16	.00375	18.9×10^{-3}	7.3×10^{-6}				
21	.00415	20.9×10^{-3}	6.7×10^{-6}				
0	.00415	21.2×10^{-3}		.19745		2500	Average strain rate
1	.00452	23.2×10^{-3}	33.3×10^{-6}				
6	.00520	26.7×10^{-3}	11.7×10^{-6}				$\dot{\varepsilon}$/sec = 9.35×10^{-6}
11	.00560	28.8×10^{-3}	7.0×10^{-6}				
16	.00625	32.7×10^{-3}	13.0×10^{-6}				
21	.00668	34.4×10^{-3}	5.7×10^{-6}				
0	.0070	36.6×10^{-3}		.19492		3000	Average strain rate
1	.0072	37.6×10^{-3}	17.0×10^{-6}				
6	.00858	45.0×10^{-3}	24.7×10^{-6}				$\dot{\varepsilon}$/sec = 21.8×10^{-6}
11	.00992	52.2×10^{-3}	24.0×10^{-6}				
16	.0110	58.0×10^{-3}	19.7×10^{-6}				
21	.0123	65.2×10^{-3}	23.7×10^{-6}				

ZR#5(continued)

Time Minutes	$\Delta\ell$ Elongation (inches)	ε Strain	$\dot{\varepsilon}$/sec. Strain Rate	L_o (inches)	A_o (square in.)	σ Stress (psi)	Remarks
0	.01260	68.8×10^{-3}		.18942		3500	Average strain rate
1	.0133	72.7×10^{-3}	65.0×10^{-6}				
6	.0169	93.4×10^{-3}	69.0×10^{-6}				$\dot{\varepsilon}$/sec = 62.3×10^{-6}
11	.0193	107.3×10^{-3}	46.3×10^{-6}				
16	.02234	125.4×10^{-3}	60.3×10^{-6}				
21	.02588	146.7×10^{-3}	71.0×10^{-6}				
0	.02588	159.0×10^{-3}		.1763		4000	Average strain rate
1	.02820	174.0×10^{-3}	250.0×10^{-6}				
2	.02990	186.0×10^{-3}	200.0×10^{-6}				$\dot{\varepsilon}$/sec = 30.0×10^{-6}
3	.03140	196.0×10^{-3}	170.0×10^{-6}				
4	.03360	211.0×10^{-3}	250.0×10^{-6}				
5	.03640	231.0×10^{-3}	330.0×10^{-6}				
6	.0414	268.0×10^{-3}	610.0×10^{-6}				
7	.0591	408.0×10^{-3}	2330.0×10^{-6}				

Table A.6

ZR#6	Conditions (†)
	Test temperature = 1000°C
	Annealing temperature = 1055°C
	Time at annealing temperature = 20 mins
	Temperature fluctuation = ±1°C
	Stabilizing time at test temp = 30 mins
	Initial grain size = 58 microns
	Final grain size = 65 microns

†All the data presented here is in the F.P.S. system. This has been done in order to avoid a loss of accuracy in converting to the S.I. units. However the output is dimensionless and hence there is no effect on the data presented in the Deformation Mechanism Maps.

ZR#6

Time Minutes	$\Delta\ell$ Elongation (inches)	ε Strain	$\dot{\varepsilon}$/sec. Strain Rate	L_o (inches)	A_o (square in.)	σ Stress (psi)	Remarks
0	.0011	3.19×10^{-3}		.2004	.00993	2000	Average strain rate
1	.0023	1.00×10^{-3}	36.5×10^{-6}				
6	.0055	9.98×10^{-3}	29.9×10^{-6}				$\dot{\varepsilon}$/sec = 4.95×10^{-6}
11	.0072	8.48×10^{-3}	5.0×10^{-6}				
16	.0086	6.99×10^{-3}	4.97×10^{-6}				
21	.0098	5.5×10^{-3}	4.9×10^{-6}				
0	.0018			.1917	.0104	2500	Average strain rate
1	.0024	6.99×10^{-3}	1239.5×10^{-6}				
6	.0050	13.56×10^{-3}	28.4×10^{-6}				$\dot{\varepsilon}$/sec = 23.69×10^{-6}
11	.0069	9.9×10^{-3}	23.9×10^{-6}				
16	.0088	27.19×10^{-3}	18.78×10^{-6}				
21	.0104	8.35×10^{-3}					
0	.0032	17.48×10^{-3}	6.5×10^{-6}	.1831	.0109	3000	Average strain rate
1	.0039	13.58×10^{-3}	$.26 \times 10^{-6}$				
6	.0085	12.80×10^{-3}					$\dot{\varepsilon}$/sec = 3.38×10^{-6}

VITA

The author was born February 2, 1952 in Rajahmundry, India. He was raised in Madras, India and attended the local public school and graduated from St. Xavier's High School, Bombay, India on May 26, 1967. In July of 1969 he entered the Indian Institute of Technology at Madras, India, and majored in metallurgy and materials science, graduating among the top 5 percent of the class in June 1974.

In the fall of 1974, Mr. Patel began his graduate study in metallurgy at Lehigh University. In July 1976 he was engaged as a metallurgist with LaBour Pump Company in Elkhart, Indiana, and received his Master of Science degree in October 1978.